

# POLITECNICO DI TORINO

Master's Degree in Automotive Engineering



Master's Degree Thesis

## Analysis of a mathematical model of a battery

Supervisors

Prof. Iustin Radu BOJOI

Candidate

Riccardo ARCURI

MARCH 2022



# Summary

Lithium-ion cells are the most diffused technology for energy storage. Their application spans from portable devices to satellites, thanks to their high energy density and specific energy.

The high diffusion of electric vehicles goes hand in hand with the need for high range, fast charge and long life for the battery pack. This concerns both usability and sustainability.

While discharging operation cannot be controlled, because depending on the amount of torque requested by the driver, the charging phase can be addressed to minimize charging time or aging, or even selecting the best trade-off of the two.

For a safe, reliable and efficient operation of the battery pack, the battery management system (BMS) monitors and controls the operation of each cell. To predict the behavior of a cell and apply the best control strategy, a model that describes the electrical operation is necessary.

Two types of models are presented. One is based on the dynamics of lithium atoms across the two electrodes, thus it is an accurate description of the real cell. The high conceptual and computational complexity makes the physics based model (PBM) intractable in this work because of the poor availability of data. The equivalent circuit model (ECM) is instead built from the analysis of variables at the terminals of the cell, namely current and voltage, and related parameters such as resistances and capacitors. The model can be improved by integrating a thermal model and an aging model.

The heat developed by the current flowing through the cell is responsible for the temperature rise. The temperature variation affects the parameters that describe the cell, thus the state of the cell is continuously updated.

Moreover, extreme temperatures accelerate undesired reactions, making it necessary to provide the battery pack with a cooling system. High current intensity for fast charging is responsible also for the aging of the cell. It leads to lithium loss, hence to a reduction in the capacity.

Although most present electric vehicles are provided with pouch cells, the three coupled models are built considering an A123 cell.

The choice comes from the lack of data about pouch cells, while analyses on the

selected cylindrical cell are available in some papers. Nevertheless, the model can be applied to any cell for which electrical, thermal and cycling data are accessible.

# Acknowledgements

I would like to thank Professor Bojoi for his support in this work.

A special thanks to Guglielmo from Teoresi for his guidance, helpfulness and continuous encouragement.

I am grateful to my family and all my friends, from those I've known since I was a child to the ones that flooded my life of happiness since few months.



# Table of Contents

<b>List of Tables</b>	VIII
<b>List of Figures</b>	IX
<b>Acronyms</b>	XII
<b>1 Introduction</b>	1
<b>2 Battery cells and battery pack</b>	3
2.1 Cell characteristics and working principles . . . . .	3
2.2 Lithium-ion cell . . . . .	6
2.3 Future of battery cells . . . . .	9
2.4 Electric powertrain . . . . .	9
2.5 Battery Management System . . . . .	11
<b>3 Models for lithium-ion cells</b>	15
3.1 Equivalent circuit model . . . . .	15
3.2 Physics based model . . . . .	18
3.3 Selection of the model . . . . .	22
<b>4 Thermal analysis and aging mechanisms</b>	24
4.1 Thermal analysis . . . . .	24
4.1.1 Temperature control . . . . .	26
4.1.2 Thermal model . . . . .	27
4.2 Degradation factors . . . . .	28
4.2.1 Solid electrolyte interphase . . . . .	29
4.2.2 Secondary reactions on SEI . . . . .	30
4.2.3 Algorithm for degradation analysis . . . . .	31
<b>5 Energetic framework</b>	33
5.1 Energetic quantities . . . . .	33
5.1.1 Pack related quantities . . . . .	33

5.1.2	Capacity . . . . .	34
5.1.3	State of charge . . . . .	35
5.1.4	Equivalent circuit model . . . . .	36
5.1.5	State of health . . . . .	36
5.2	Data collection . . . . .	37
5.3	Estimation algorithms . . . . .	39
<b>6</b>	<b>Model definition</b>	<b>45</b>
6.1	Heat generation and temperature variation . . . . .	46
6.2	Capacity loss . . . . .	49
6.3	Electrical model . . . . .	50
<b>7</b>	<b>Results</b>	<b>51</b>
7.1	Dataset used for the model . . . . .	51
7.2	Outcomes of the simulations . . . . .	53
7.2.1	2C at 25 °C . . . . .	54
7.2.2	3C at 25 °C . . . . .	57
7.2.3	5C at 25 °C . . . . .	60
7.2.4	Test replicated from article . . . . .	61
7.3	Battery pack . . . . .	62
7.4	Future works . . . . .	63
7.4.1	Kalman filters for SOC and SOH estimation . . . . .	63
7.4.2	Balancing of pack cells . . . . .	64
7.4.3	Charging strategies and control . . . . .	64
<b>8</b>	<b>Conclusions</b>	<b>67</b>
<b>A</b>	<b>Matlab scripts</b>	<b>69</b>
A.1	Open circuit voltage and ohmic resistance . . . . .	69
A.2	Thermal-aging-electrical model . . . . .	70
	<b>Bibliography</b>	<b>76</b>

# List of Tables

2.1	Standard potentials of electrode reactions at 25 °C . . . . .	6
7.1	A123 cell thermal parameters . . . . .	53
7.2	Parameters for computing the capacity loss for different C-rates . .	53

# List of Figures

2.1	Pouch (a), cylindrical (b) and prismatic (c) cells types. . . . .	4
2.2	Lead acid battery chemical reactions diagram [6]. . . . .	5
2.3	Electrode crystal structure in which $\text{Li}^+$ ions intercalate through the 1-D (c), 2-D (a), and 3-D (b) frameworks [10]. . . . .	8
2.4	Components of a lithium-ion cell and its operation [13]. . . . .	8
2.5	Diagram of an electric vehicle. . . . .	10
2.6	Diagram of BMS modules. . . . .	11
2.7	Diagram of battery pack connection and contactors. . . . .	12
2.8	Current-temperature (a) and voltage-temperature (b) protection mechanisms design [18]. . . . .	14
3.1	Relation between OCV and SOC for different cells chemistries (a) and relative equivalent circuit (b) [13]. . . . .	16
3.2	Equivalent circuit with ohmic resistance [13]. . . . .	16
3.3	Voltage response to a discharge pulse and effects of the lithium diffusion (a) and equivalent circuit with one RC pair (b) [13]. . . . .	17
3.4	Voltage variation during charging and discharging due to hysteresis (a) and equivalent circuit that includes hysteresis modeling (b) [13]. . . . .	17
3.5	Diagram of the ECM and PBM approaches for modeling lithium-ion cells. . . . .	18
3.6	Particles and electrolyte inside a small volume of the electrode [13]. . . . .	20
3.7	Schematic of the P2D electrochemical model of a cell [23]. . . . .	21
3.8	Variables relative to positive and negative electrodes and separator [24]. . . . .	22
4.1	Variation of different cell parameters with respect to temperature [13]. . . . .	25
4.2	Example of cooling system of a battery pack [38]. . . . .	26
4.3	Example of "second life" application of battery packs [44]. . . . .	28
4.4	Diagram of SEI formation on the electrode surface [18]. . . . .	30
4.5	SEI growth because of electrode particle cracking [18]. . . . .	31
4.6	Secondary processes on the surface of the electrode material. . . . .	31

5.1	Visualization of the different capacity definitions. [55]	34
5.2	State of charge of the cell compared to the average lithium concentration in the negative electrode [18].	35
5.3	Current shunt for measuring battery current.	37
5.4	Current pulse and voltage response for computing cell parameters.	39
5.5	SOC as function of OCV for six lithium-ion chemistries.	40
5.6	Diagram of the model-based estimation approach.	40
5.7	Diagram of the sequential probabilistic inference concept.	42
6.1	Diagram of the interactions between thermal, degradation and electrical models.	46
6.2	Diagram of the thermal model of the battery cell [61].	47
6.3	MATLAB Function implemented on Simulink to model temperature evolution.	48
7.1	OCV and ohmic resistance variations from online datasheet.	52
7.2	OCV and ohmic resistance variations from online articles.	52
7.3	Voltage and temperature evolution during charging at different C-rates [65].	54
7.4	Temperature variation during 2C charging simulation at 25 °C.	55
7.5	Ohmic resistance variation during 2C charging simulation at 25 °C.	55
7.6	SOC and cell terminal voltage variation during 2C charging simulation at 25 °C.	56
7.7	SOH variation during 2C charging simulation at 25 °C.	57
7.8	Temperature variation during 3C charging simulation at 25 °C.	58
7.9	Ohmic resistance variation during 3C charging simulation at 25 °C.	58
7.10	SOC and terminal voltage variation during 3C charging simulation at 25 °C.	59
7.11	SOH variation during 3C charging simulation at 25 °C.	59
7.12	Test conducted at different C-rate with resulting temperature and SOC increase [64].	60
7.13	Temperature, SOC and voltage evolution for a test at 5C.	60
7.14	Test for the minimum charging time [64].	61
7.15	Temperature, SOC and voltage evolution for the replicated test.	61
7.16	SOC variation during 1C charging simulation at 25 °C for the battery pack.	63
7.17	SOC evolution with imbalanced cells.	64
7.18	Balancing strategy for battery pack cells [66].	65
7.19	Multilevel constant current charging strategy [68].	66
7.20	Pareto frontier to evaluate the incidence of the weighting factor on charging time and degradation [64].	66



# Acronyms

**OCV**

open circuit voltage

**SOC**

state of charge

**SOH**

state of health

**SOL**

state of life

**BMS**

battery management system

**ECM**

equivalent circuit model

**PBM**

physics based model

**SPM**

single particle model

**P2D**

pseudo-two dimensions

**ODE**

ordinary differential equation

**PDE**

partial differential equation

**SEI**

solid electrolyte interphase

# Chapter 1

## Introduction

To contain the increasing global warming and the other consequences of climate change, COP26 signed the agreement to achieve carbon neutrality by 2050. Energy transition is a fundamental strategy to achieve the goal, by means of decarbonization, electrification of transports and switching to a cleaner energy production through renewables. A report from IEA [1] points out that the transport sector is responsible for 24 % of the global CO<sub>2</sub> emissions. In detail, 74.5 % of CO<sub>2</sub> emissions in the transport sector are due to road vehicles. More efficient internal combustion engines, enabled mainly by combustion control, and devices for reducing the emissions at the tailpipe, allow a reduction of CO<sub>2</sub> and other pollutants such as NO<sub>x</sub>. Notwithstanding the improvement, the increasing demand for passenger cars lead to a rise in the emission of greenhouse gasses (GHG) up to 2018 [2]. On the other hand, while total car sales in 2021 reduced by 25 % with respect to 2019, a sharp increase was registered in the electric vehicle market. For instance, EVs sales in Europe reached a value of about 1.1 million in 2021. In [3] is reported an increase of 70 % of the sales of pure electric vehicles and PHEV (plug-in electric vehicles) together. The electric vehicle market results as the most dynamic among the players of clean energy. Since it is not provided with an internal combustion engine, an EV offers opportunities of reducing GHG and other pollutants emissions, at least locally (Tank to Wheel, or TTW). Anyway, the growth of the share of electricity produced by renewables, also solves the problem of pollution from energy generation plants (Well to Tank, or WTT). Beside the vehicle usage, the sustainability of an electric vehicle must be evaluated on the entire life of the vehicle, starting from the provision of raw materials and production to the end of life and recycling. This process is defined as “life cycle assessment” (LCA). The production of the battery is responsible for over 40 % of CO<sub>2</sub> emission considering all the production of an electric vehicle [4]. Lithium is an abundant element on Earth, but its extraction is a high energy consuming process. What is more rare is the cobalt, furthermore more than half of cobalt world’s supply is extracted in the Democratic Republic of

Congo, where miners (even children) work in hazardous conditions. For this reason, cobalt is more and more substituted in new compounds, as in LFP cells. At the end of life, a crucial question is the disposal of the battery packs, also considering the increasing diffusion of electric vehicles. Thus, the recycling of battery cells is fundamental for sustainability. Elements can be recovered and reused for producing new electrodes, with the goal of 95 % recovery of lithium, nickel and cobalt in the next years [5]. To postpone the end of life, the aging mechanisms must be known, so the cell's operation can be controlled to minimize the degradation. A model of battery behavior can be also useful for avoiding oversizing of the battery pack and at the same time maximizing the performance of the system. The electrical model is built using an equivalent circuit and it is improved by incorporating a thermal model and an aging model.

# Chapter 2

## Battery cells and battery pack

This chapter covers battery cells basics, their characteristics and their operating principles, for different chemistries. A focus is dedicated to the lithium-ion technology, being the most diffused one for automotive applications. The powertrain of an electric vehicle is introduced, with a deepening on the battery management system whose functionalities illustrated.

### 2.1 Cell characteristics and working principles

The cell is the elementary unit of a battery pack. It delivers a voltage that depends on the chemistry of the electrodes and on the operating conditions, such as the state of charge or the temperature.

A battery cell can store a certain quantity of charge, that can be delivered to an external circuit. The maximum quantity of charge that can be held by a cell is named nominal charge capacity. The quantity of charge can be restored by recharging the battery, in case of secondary cells, while we deal with primary cells if they are single use. A relative measure of the current is the C-rate, that is the constant current that should enter/exit the cell for 1 h to completely charge/discharge the cell.

Energy is stored under the form of electrochemical energy and delivered as electrical energy when a load is connected. Research is trying to increase the values for specific energy and the energy density, to have lighter and smaller batteries: the specific energy defines the maximum amount of energy that can be stored per unit weight, the energy density is referred to the unit volume.

Cells can be connected in series or in parallel, to obtain a high-voltage or high-capacity battery, respectively. More cells connected, form a battery module. Again,

more modules can be wired to obtain a battery pack. Cells can have different shapes: cylindrical, prismatic or pouch. For the first two types, the positive and negative electrodes are constituted by a long foil with the separator in between and wound around a mandrel. Pouch cells present instead a stacked structure of alternated positive and negative electrodes, with the separator on every electrode layer. Prismatic and pouch cells can better exploit the available space, while the spacing in between the cylindrical cells helps the thermal management.

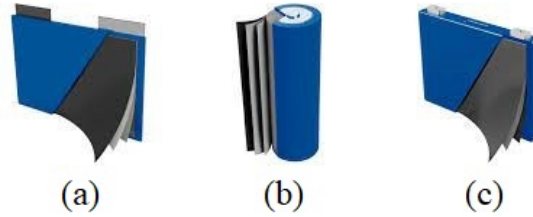
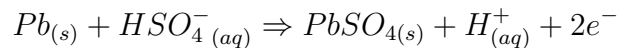


**Figure 2.1:** Pouch (a), cylindrical (b) and prismatic (c) cells types.

The components of a cell are a positive and a negative electrode and the relative current collectors, the electrolyte, and the separator. The positive and negative current collectors are the connection point with the external circuit. Charging and discharging processes are possible thanks to redox reactions. The negative electrode is the region of the cell where the charge is accumulated: during discharging electrons are released towards the external circuit through an oxidation reaction. Because of this reaction, the negative electrode is also defined as anode. Electrons arrive at the positive electrode (cathode) where a reduction reaction occurs. During charging, electrons are forced from the positive electrode to the negative one, which are now named anode and cathode respectively. The electrolyte is necessary to allow ions transfer from one electrode to the other, while the separator electrically isolates the two electrodes to avoid short circuit but still is a good conductor for ions.

In a lead-acid cell, the negative electrode is made of lead ( $Pb$ ), the positive one is made of lead dioxide ( $PbO_2$ ) and the electrolyte is a solution of water and sulfuric acid ( $H_2SO_4$ ). During discharge, the lead of the negative electrode reacts with the  $HSO_4^-$  in the electrolyte: 2 electrons are released to the external circuit, a hydrogen ion is released into the electrolyte and solid lead sulfate ( $PbSO_4$ ) forms as crystals on the electrode surface.



On the positive electrode, the lead dioxide ( $PbO_2$ ) of which it is constituted, reacts with the electrons coming from the external circuit, the hydrogen ions and

$HSO_4^-$  present in the electrolyte, again forming solid lead sulfate on the electrode surface and releasing water.

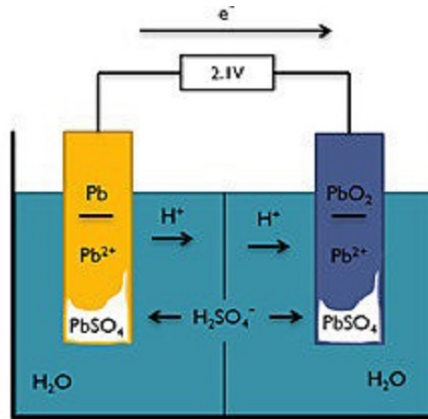
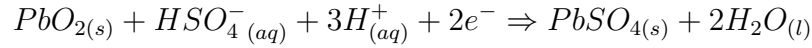


**Figure 2.2:** Lead acid battery chemical reactions diagram [6].

The potential difference across the two terminals of the cell is named electromotive force because it is the cause of electrons motion. It depends on the materials of the two electrodes.

The potential of the electrodes is calculated considering a standard hydrogen electrode as reference, for which  $2H^+ + 2e^-$  spontaneously converts to  $2H$  at “zero volts”. To obtain a large potential between the electrodes, a low (possibly negative) electrode potential for the negative electrode should be selected and a higher potential for the positive electrode. On a periodic table, strong reducing elements are found on the left and strong oxidizing elements on the right. The most reactive atoms are those that present one or two valence electrons on the outer shell or that miss one or two electrons on the outer shell.

Selecting lithium and fluorine as materials for the two electrodes, their standard potentials ( $E^0$ ) are respectively -3.04 V and 2.87 V as reported in table 2.1, resulting in a cell voltage of 5.91 V. This electrochemistry cannot be adopted because the voltage is too high to be sustained by the known electrolytes [7].

For a lead-acid battery cell, the negative electrode has a standard potential -0,356 V, the positive electrode standard potential is 1.685 V. The result is a cell potential of 2.05 V, that varies with the variation of sulfuric acid concentration. In fact, a discharged cell presents a high quantity of lead sulfate deposited on the electrodes surface and almost no sulfuric acid in the electrolyte because of the reactions with the electrodes material. To obtain a 12 V battery, six lead acid cells (2 V each) are put in series [8].

Alternatively to the cell chemistries involving redox reactions, some metallic alloys are capable of storing hydrogen (insertion) as a sponge can store water. The chemical structure of the electrode does not change, even if some small increase in the volume can be observed, resulting in a very long life of the cell. On the other hand the cell potential is lower (1.3 V) than a lead acid cell. These compounds are called metal hydride and present in NiMH and NiCd cells.

Reduction half-reaction	Standard Potential
$Li^+ + e^- \Rightarrow Li_{(s)}$	-3.04
$K^+ + e^- \Rightarrow K_{(s)}$	-2.92
$Ca^{2+} + 2e^- \Rightarrow Ca_{(s)}$	-2.84
$Na^+ + e^- \Rightarrow Na_{(s)}$	-2.71
$Zn^{2+} + 2e^- \Rightarrow Zn_{(s)}$	-0.76
$2H^+ + 2e^- \Rightarrow H_{2(g)}$	0.00
$Cu^{2+} + 2e^- \Rightarrow Cu_{(s)}$	0.34
$O_{3(g)} + 2H^+ + 2e^- \Rightarrow O_{2(g)} + H_2O_{(l)}$	2.07
$F_{2(g)} + 2e^- \Rightarrow 2F^-$	2.87

**Table 2.1:** Standard potentials of electrode reactions at 25 °C

## 2.2 Lithium-ion cell

Lithium-ion cells have a similar operation principle to metal hydride cells, not involving redox reactions of the lithium with the electrodes material.

During discharging, lithium atoms exit the negative electrode and split in an electron that runs across the external circuit, and the lithium ion that reaches the positive electrode through the electrolyte.  $Li^+$  and  $e^-$  join at the positive electrode and fill the vacant spaces between the electrode particles, diffusing to equalize the concentration.

The operation of lithium atoms entering the structure of the electrode is called intercalation. When charging a cell, we have the opposite process, with lithium ions that exit the positive electrode (deintercalation).

Li-ion cells are capable of higher specific energy and energy density, lower self-discharge and longer life thanks to the gentler intercalation mechanism with respect to redox reactions. On the other hand, they are more expensive and complex to produce.

The negative electrode is generally made up of layers of graphite (graphene), kept together by a loose bond, so that lithium ions can easily intercalate. Each graphite site, constituted by six carbon atoms, can hold an atom of lithium. Lithium titanate is an alternative for the negative electrode: the absence of side reactions allows faster charging and longer lifetime, but the high electrode potential results in a low energy density.

A much higher energy density is enabled by the use of silicon: a single silicon atom can house four lithium atoms, but this leads to a huge volume change: the electrode material tends to fracture because of the cyclic expansion and contraction during charging and discharging.

Battery cell typologies are generally named after the compounds used for the positive electrode because of the high variety. They can be grouped according to their structure:

- 2-D structures host lithium atoms in between the layers as represented in figure 2.3(a). For LCO ( $Li_xCoO_2$ ), a quantity  $x$  of lithium between 0.5 and 1 is needed to avoid fast aging. Since cobalt is rare and toxic, a portion can be substituted by nickel, which confers a higher energy density to the cell and its poor thermal stability can be mitigated by the manganese, as in NCM cells. NCA cells blend instead nickel, cobalt and aluminum.
- a 3-D diffusion of lithium occurs in cubic spinel structures like the ones of figure 2.3(b), such as in LMO ( $Li_xMn_2O_4$ ) electrodes. They are inexpensive and non-toxic, but they easily degrade [9].
- LFP ( $Li_xFePO_4$ ) electrodes present olivine structure (1-D) as figure 2.3(c), where lithium intercalates in linear tunnels. They are not expensive but the energy density is low because of the presence of iron. Moreover, it is difficult to estimate the SOC due to the cell potential that is constant for about 80 % of the lithium variation.

To withstand voltages higher than 2 V, non aqueous organic solvents are used, such as ethylene and propylene carbonates (cyclic type) or dimethyl, ethyl methyl and diethyl carbonates (linear). New applications include fluorinated organic solvents and solvents containing boron or sulfur [11]. Salts are used to increase the ionic conductivity and they do not take part in the chemical reactions. Lithium hexafluorophosphate ( $LiPF_6$ ) is the most used. Some products of the decomposition of solvents and salts lead to formation of the solid electrolyte interphase (SEI), which is an electrically insulating layer but does not affect the ionic conductivity, and it prevents further reaction of the solvent with the graphite contained in the electrode. Additives are used to control the formation of SEI, to avoid thermal runaway, to protect from overcharge and to act as flame retardant [12].

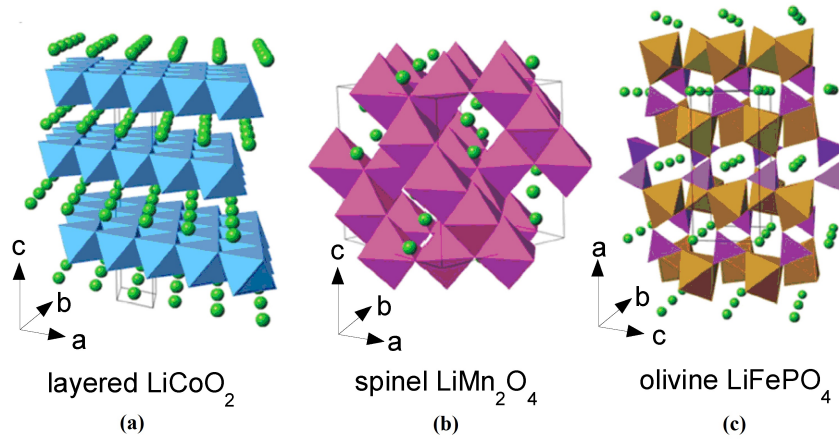


**Figure 2.3:** Electrode crystal structure in which  $\text{Li}^+$  ions intercalate through the 1-D (c), 2-D (a), and 3-D (b) frameworks [10].

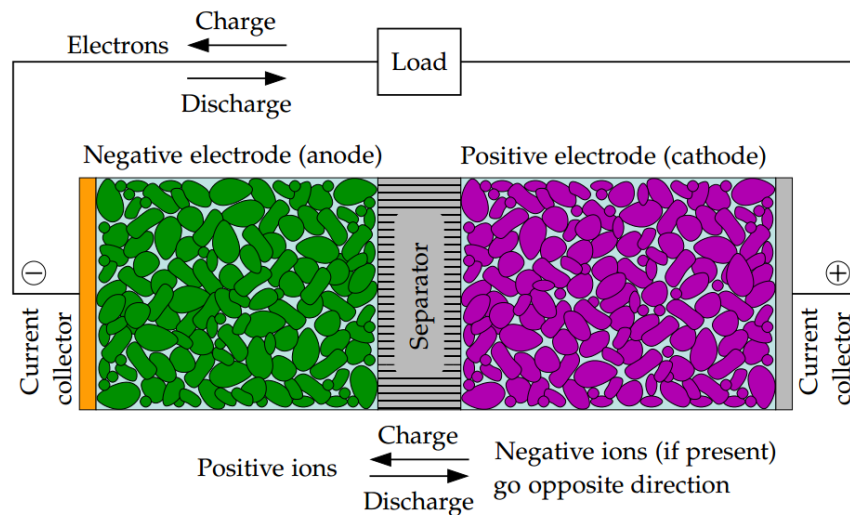


**Figure 2.4:** Components of a lithium-ion cell and its operation [13].

A cell can fail because of errors during the design or manufacture processes, or during use because of uncontrolled operations, abuse or aging.

Corrosion, SEI formation and growth of crystals, called dendrites, lead to aging, with the result of reduced capacity and increased internal impedance and self-discharge.

## 2.3 Future of battery cells

Research on energy storage technology is pushed by the increasing demand of EVs and by the requirements on their performances. The need for high range and fast charging time implies high specific energy and energy density, resistance to high currents and temperatures.

Present batteries for automotive application offer energy density very close to 600 Wh/l and specific energy of about 250 Wh/kg at cell level. Obviously, when considering the battery pack, the two values will be lower, because of the added materials and the required space to assembly all the cells together, not contributing to the energy storage.

Appetible because of its high energy density, to enable the use of silicon in the negative electrode structure, Nanowire technologies help in controlling the volume change during intercalation and deintercalation, hence to increase the cell lifespan [14].

Another promising type of battery cells, is the Zinc-air, which presents a zinc anode and an air cathode. The design of the cell is based on the It features low cost and very high specific energy (about 1000 Wh/kg). Electrolytes inspired by processes relative to the human breathing system, increase ionic conductivity and dimensional stability, with the result of better performances and extended cycle-life [15].

The development of solid state electrolytes is pushed by the need to overcome the limitations of liquid electrolytes, such as high decomposition at high voltages, resistivity of the SEI and risk of thermal runaway. Since the solid electrolyte do not suffer decomposition, high voltages and high temperatures can be reached, thus the cooling system serves no purpose, leading to money savings [16].

## 2.4 Electric powertrain

The powertrain of an electric vehicle includes the battery pack, power electronics devices and the electric motor. A vehicle can be provided with one or more electric motors, even one each of the wheels. The connection between the electric motor and the wheels is in charge of the transmission, which generally features a fixed reduction ratio for the gearbox, since the electric motor is able to cover a wide range of rotating speeds. The electric motor presents a constant torque zone and a constant power zone. The first is limited by the current that flows through the power electronics, the second depends on the maximum rotating speed of the motor.

Between the electric motors and the battery pack, some devices are required to convert the DC power provided by the battery into AC power to be delivered to

the electric motor, or the opposite, namely to convert the AC power developed by the motor during the "regenerative braking" into DC power to recharge the battery.

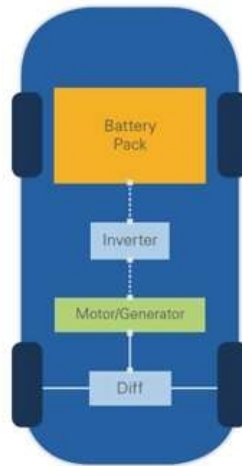


**Figure 2.5:** Diagram of an electric vehicle.

The first operation described is performed by the inverter, that is able to generate a sinusoidal wave for the voltage, as required by the electric motor. The component at the base of the inverter operation is the switch, that controls the conduction across a certain circuit. By cyclically varying the duty cycle of the switch, that is the percentage of the switching period during which the device is ON, the mobile mean value of the voltage assumes a sinusoidal profile.

The rectifier instead executes the reverse operation, by selecting as output the actual maximum of the three voltages produced by the electric motor, hence delivering to the battery pack an almost constant voltage, at least not periodical.

Another device is the DC-DC converter, that reduces the high voltage of the battery to be applied to the inverter, or amplifies the voltage produced by the rectifier to feed the battery.

The energy path that goes from the battery to the wheels, or the way back, is not fully efficient. Each step presents some electrical or mechanical losses. Power electronics present switching and conduction losses, so the conversion efficiency of the devices is generally as high as 95÷98 % and the mechanical efficiencies of the transmission and the electric motor are higher than 90 %.

The traction system includes some components that support the battery pack operation.

To disconnect the battery pack from the load when not in use, two high-current capable relays, called contactors, are used. A third pre-charge contactor is needed to avoid big currents when closing the two main contactors, in case the load has

capacitive nature. Also fuses are present to isolate the battery in case of problems during charge or in the event of a crash.

Since the temperature of each cell must be maintained within a certain range, a dedicated system is included in the battery system. This issue is investigated in section 4.1.

The mentioned DC-DC converter connects the high voltage battery pack also to a 12 V circuit. It includes the auxiliaries, that is to say lights, windows, power steering and brakes, passenger compartment air conditioning and others, and the related 12 V battery.

Finally a control unit is essential to coordinate the different players on the basis of the actual or the predicted state of the battery system. This is the aim of the battery management system.

## 2.5 Battery Management System

The battery management system (BMS) is an embedded system to properly manage a battery pack, so it includes both hardware and software parts.

The chipset must be selected according to the number of cells to be monitored, if active or passive balancing is used, required accuracy and points of temperature measurement and most of all cost. The BMS has a hierarchical design: it features a master, which controls the contactors between battery pack and load and the thermal management, and communicates with BMS slaves, which are welded to the modules to minimize wiring. They have to measure the voltage of each cell of the module and to balance the energy.

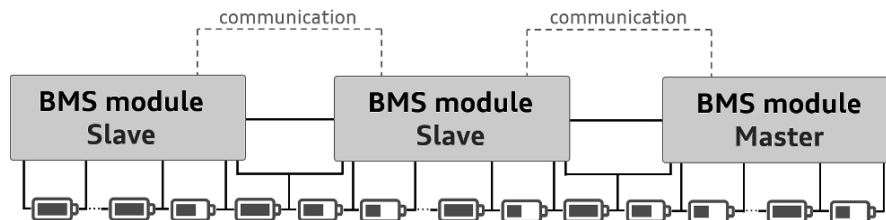


**Figure 2.6:** Diagram of BMS modules.

Some purposes of the BMS are to protect the operator in case of maintenance and to protect the cells in case of damage or failure. It can prolong the battery life by controlling the power limit and avoiding overcharge and overdischarge, while guaranteeing the functional design requirements.

The functionalities of the BMS are:

- measurement of voltage, current and temperature,

- protection from abuse,
- interface,
- performance management,
- diagnostics.

The voltage of each cell is needed for balancing, for estimating SOC and SOH and for safety, so as to avoid overcharge. The basic voltage measurement is performed using analog-to-digital converters (ADC).

The temperature affects some operational characteristics such as the internal resistance, and can cause some unwanted events such as the lithium plating when charging at low temperature. Cell internal temperature can be estimated through an accurate model, while sensors can be placed on the module.

The current cannot be measured directly, but computed from a voltage measurement, by means of two devices. A resistive shunt current sensor measures the voltage not at the connection terminals, but in correspondence of small screws, where a certain resistance is calibrated. The other device exploits the Hall effect: a coil is wrapped around the wire where the current needs to be measured flows, obtaining a second current that is induced in the coil. There is no direct electrical connection, but a feedback circuitry is needed to check magnetic hysteresis.

The BMS is in charge of controlling the contactors, so the connection of the battery pack with the load. The negative contactor is the first to be closed, then the pre-charge contactor allows the current to rise gradually thanks to its resistance. As this current is close enough to the battery pack current, the positive contactor is closed and the pre-charge one is opened.

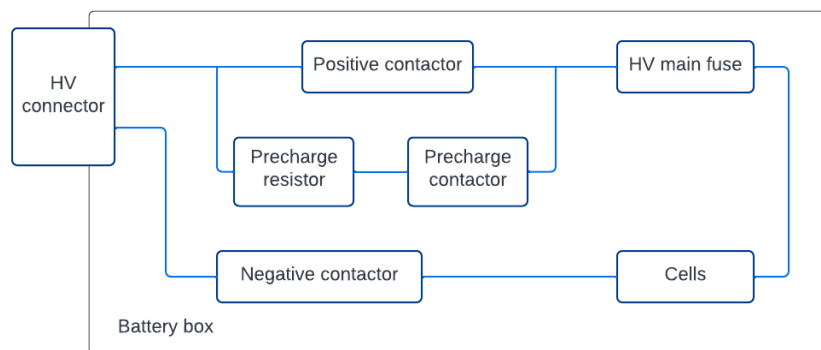


**Figure 2.7:** Diagram of battery pack connection and contactors.

While for a 12 V battery it is safe to ground it to the vehicle chassis to reduce wiring, a battery pack must be well isolated: according to FMVSS a current lower

than 2 mA is safe for human body, which means that the isolation resistance between battery pack and vehicle ground must be greater than 500 times the battery voltage [17]. The BMS needs to check the isolation resistance.

As mentioned, temperature affects some cell parameters and is responsible for some degradation mechanisms. Overcharge causes a temperature rise in the cell, moreover if done at low temperature, it leads to lithium plating. The growth of the SEI layer causes further thermal isolation and so temperature rises. Short circuits can occur when the separator melts due to high temperatures, enabling high currents. The heat that generates induces the breakdown of the electrolyte and the formation of gasses that are flammable. A uniform aging of the cells can be obtained keeping a uniform temperature across the battery pack. Cells can be warmed up when temperature is too low to avoid damage. Thermal management can be performed using air cooling or liquid cooling.

The BMS has to ensure that all the cells work in the safe operating region considering voltages, currents and temperatures and the protection circuit must react quickly in case of short circuit or uncontrolled release of energy. Faults can be detected by the BMS slaves, which are able to disconnect the pack and their communication with the master needs to be very quick and free of electro-magnetic interferences. When one or more cell parameters are in the “failure zone” (specified by the cell manufacturer) of figure 2.8(a), the cell is permanently damaged.

The safe operating zone is described by a certain temperature value as in figure 2.8(b), over which the thermal fuse disconnects the pack, a threshold in the current value, checked by the electronic protection and a function of the two parameters: the resettable fuse disconnects the pack until the current and the temperature decrease again in the safe operating zone. Electronics also monitor the voltage values and the battery is disconnected in case of overvoltage for the battery or the charger, or undervoltage for the battery or the load. All the events that are out-of-tolerance are recorded, together with their duration.

Communication in the automotive environment requires a robust protocol because of the high quantity of electrical noise. The CAN (Controller Area Network) protocol manages the messages to be exchanged between the processors, the priority and sequence, and the transmission speed, that is high (1 Mb/s) for critical operations such as engine management, or low (100 kb/s) for operations such as switching lights or opening the windows. Messages are packets of about 60 bits divided in fields, according to the different information to be transmitted.

To allow a proper management of the performances of the battery pack, for instance the available energy and the instantaneous available power, cells SOC, capacities and resistances must be estimated. Poor estimation methods abruptly correct overcurrent or overvoltage events and force an overdesign of the pack to make up for the uncertainties.

A model of the battery pack can be intergrated into the BMS software to monitor

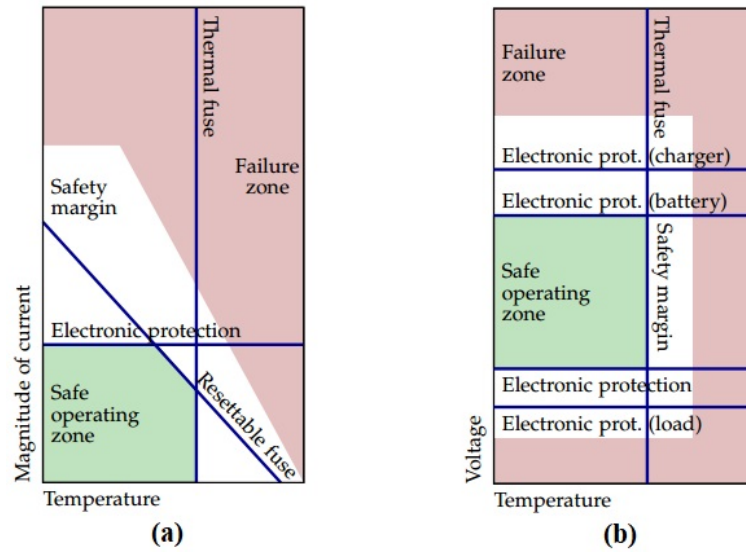


**Figure 2.8:** Current-temperature (a) and voltage-temperature (b) protection mechanisms design [18].

or even to predict the state of each cell, starting from the variables that can be measured or estimated, which are current, voltage and temperature. Once the present or future state is known, the proper control of the battery can be applied to comply with driver request and respecting the battery system limits.

## Chapter 3

# Models for lithium-ion cells

In this chapter the two main models to predict the behavior of a cell are presented.

The first is based on empirical observations, which means on the parameters that can be measured at the cell terminals. It is not a description of the cell's internal components and internal behavior and for this reason it is not capable of predicting the degradation of the cell.

The second model is based on physics, so on the electrochemical mechanisms that occur inside the electrodes. Hence the latter is more accurate and is able of predicting the behavior considering all the possible reactions that occur inside the electrodes or electrolyte materials.

### 3.1 Equivalent circuit model

This model is built using simple electrical elements that approximate the cell behavior.

Starting from the simplest description of a cell, it can be modeled as a voltage generator. Actually, the voltage that is registered at the cell's terminal when it is fully charged, is higher than the voltage measured when the cell is discharged. The first improvement is the relation of the open circuit voltage with the state of charge, (defined with  $z$ ) of the battery cell. The coulombic efficiency can be included in the formulation to account for the quantity of charge that does not enter the cell because of side reactions. The relation between OCV and SOC varies according to the cell chemistry and the temperature.

$$\dot{z}(t) = -\frac{\eta(t)i(t)}{Q} \quad (3.1)$$

When the cell is charging, the measured voltage is slightly higher than the OCV at the same SOC, while it is lower when a load is connected and the cell

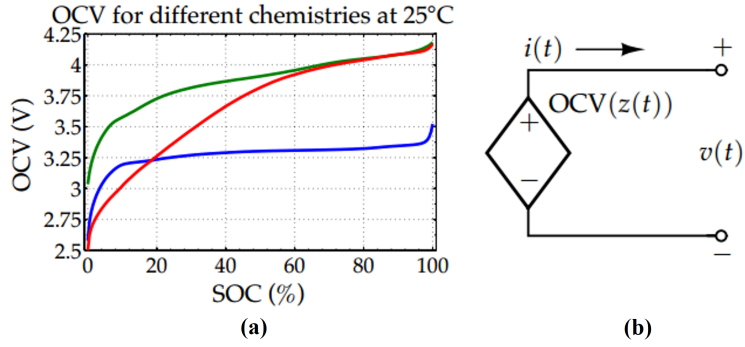


**Figure 3.1:** Relation between OCV and SOC for different cells chemistries (a) and relative equivalent circuit (b) [13].

is discharging. This effect can be modeled by adding a resistance in series to the circuit, so the voltage at the terminal is:

$$v(t) = OCV(z(t)) - R_0 i(t) \quad (3.2)$$

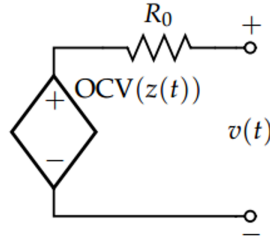


**Figure 3.2:** Equivalent circuit with ohmic resistance [13].

When looking at the voltage behavior as a result of a current pulse, it can be noticed an instantaneous voltage drop as the load is connected, then the voltage decreases at a much lower rate. As the load is disconnected, after an instantaneous increase the voltage stabilizes within some time. This effect is due to the diffusion of lithium atoms inside the electrodes, which is a slow process.

An infinite series of RC pairs, defined as Warburg impedance, can be used to model it. Actually, one or few RC pairs are enough to provide a good model, as a trade off between accuracy and simplicity: one RC circuit models the short time constant and a second one models the long time constant. The two can be included in the model, so the diffusion voltage is added to the voltage equation.

Equations 3.3 and 3.4 and figure 3.3 are now reported for a model that includes just 1 RC pair.

$$\frac{di_{R_1}(t)}{dt} = -\frac{1}{R_1 C_1} i_{R_1}(t) + \frac{1}{R_1 C_1} i(t) \quad (3.3)$$

$$v(t) = OCV(z(t)) - R_1 i_{R_1}(t) - R_0 i(t) \quad (3.4)$$

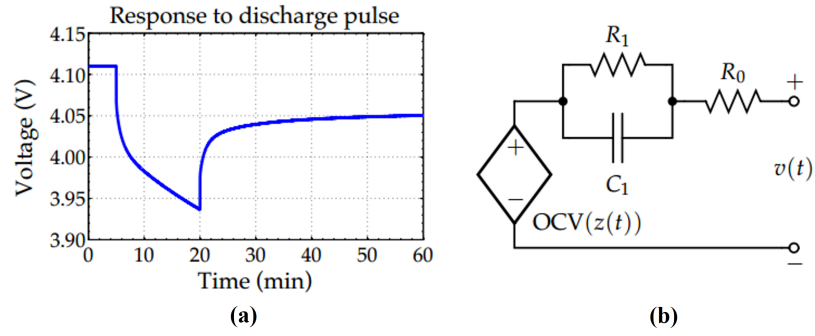


**Figure 3.3:** Voltage response to a discharge pulse and effects of the lithium diffusion (a) and equivalent circuit with one RC pair (b) [13].

Another drift from the OCV is due to the hysteresis, but in this case there is not any voltage recovery as time flows. This means that, as the cell rests, hysteresis voltages do not change, while diffusion voltages decrease to zero. Hysteresis is due to mechanical stress, caused by the intercalation and deintercalation processes of lithium in the electrodes. Also, thermodynamic effects participate to the hysteresis, because related to the energy of particles and so to the insertion rate of lithium in the electrodes [19].

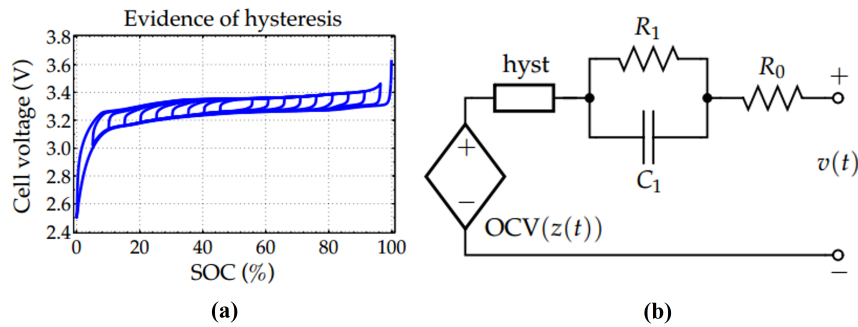


**Figure 3.4:** Voltage variation during charging and discharging due to hysteresis (a) and equivalent circuit that includes hysteresis modeling (b) [13].

The variation of the dynamic hysteresis voltage  $h(z, t)$  as function of the SOC is given by

$$\frac{dh(z, t)}{dz} = \gamma \text{sgn}(\dot{z})(M(z, \dot{z}) - h(z, t)) \quad (3.5)$$

where  $\gamma$  is index of the rate of change of the hysteresis with respect to SOC and  $M(z, \dot{z})$  is the maximum polarization due to hysteresis, that is positive for charging because the SOC increases.

### 3.2 Physics based model

Since equivalent circuit models are not constructed considering the real components of a cell, they are not capable of modeling many of the mechanisms that occur in the device.

The possibility of simulating those mechanisms enables the batteries to operate at their physical limits [20]. The intercalation of lithium atoms in the electrodes can be simulated under all possible conditions of temperature and current rate, so eventual secondary reactions or damages to the electrodes structure can be predicted. Hence an electrochemical model that is based on physics is able to have an updated description of the cell as it ages because of lithium consumption or active material dissolution [21]. If the internal state of the cell is known, the BMS can operate the battery so that degradation is minimized [22].

PBMs are very complex, both conceptually and computationally, but they can be reduced to a form that requires the same computational power as ECMs. The construction of the model starts from the smallest scale, then the model is progressively simplified as a bigger scale is considered.

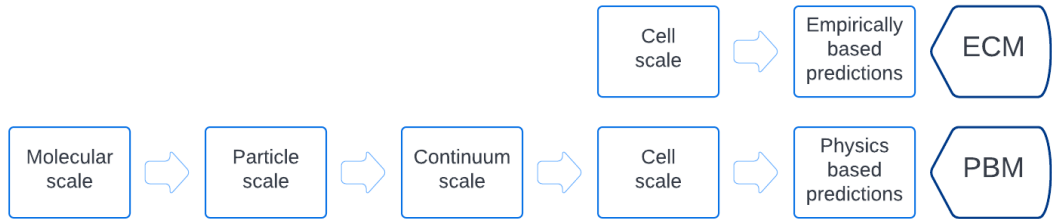


**Figure 3.5:** Diagram of the ECM and PBM approaches for modeling lithium-ion cells.

The smallest scale is called molecular scale, where processes at the atomic level are analyzed, such as those that influence the OCV and the diffusion of lithium atoms. Actually OCV and lithium diffusivity can be easily measured. At this scale are derived the partial differential equations (PDE) that describe the dynamics

and kinetics of a lithium-ion cell: the mass and charge conservation equations for both the electrode and the electrolyte and the lithium exchanged between solid and electrolyte in terms of flux density, known as Butler-Volmer equation.

The charge conservation equation in the electrode material is defined by

$$\nabla \cdot i_s = \nabla \cdot (-\sigma \nabla \phi_s) = 0 \quad (3.6)$$

where  $i_s$  is the current density in the solid material,  $\sigma$  is the bulk conductivity and  $\phi_s$  is the electric potential in the electrode.

The mass conservation in the electrode material is defined by

$$\frac{\partial c_s}{\partial t} = \nabla \cdot (D_s \nabla c_s) \quad (3.7)$$

where  $c_s$  is the lithium concentration in the electrode material and  $D_s$  is the material diffusivity.

The mass conservation in the electrolyte is instead defined by

$$\frac{\partial c_e}{\partial t} = \nabla \cdot (D_e \nabla c_e) - \frac{i_e \cdot \nabla t_+^0}{F} - \nabla \cdot (c_e v_0) \quad (3.8)$$

where this time the lithium concentration, diffusivity and current density are referred to the electrolyte material.  $F = 96485 \text{ Cmol}^{-1}$  is the Faraday's constant,  $t_+^0$  is the rate at which cations are transferred with respect to the solvent and  $v$  is the velocity of the specie.

The charge conservation in the electrolyte is given by

$$\nabla \cdot i_e = \nabla \cdot \left( -K \nabla \phi_e - \frac{2KRT}{F} \left( 1 + \frac{\partial \ln f_{\pm}}{\partial \ln c_e} \right) (t_+^0 - 1) \nabla \ln c_e \right) = 0 \quad (3.9)$$

where  $K$  is the ionic conductivity and  $f_{\pm}$  is the mean molar activity coefficient.

Last equation is the lithium exchange between solid and electrolyte materials:

$$j = \frac{i_0}{F} \left\{ \exp \left( \frac{(1-\alpha)F}{RT} \eta \right) - \exp \left( -\frac{\alpha F}{RT} \eta \right) \right\} \quad (3.10)$$

where  $\alpha$  is a charge transfer coefficient and  $\eta$  is the reaction overpotential.

For all the equations ( $\nabla$ ) and ( $\nabla \cdot$ ) operators are respectively the gradient and divergence operators.

Next step is the particle scale, where small volumes are considered. Particles representing the solid electrode material are present in the volumes, while the void between the particles is filled up by the electrolyte, both parts considered as homogeneous materials. The geometry of the particles and of the volume needs to be defined, considering that some particles are truncated by the cube surfaces.

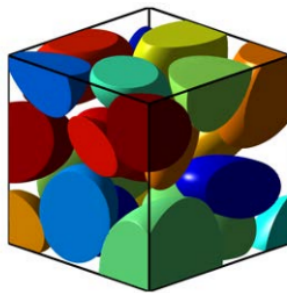


**Figure 3.6:** Particles and electrolyte inside a small volume of the electrode [13].

Mass and charge conservation equations are applied to both solid particles and electrolyte, while boundary conditions need to be defined at the interface between solid and electrolyte and at the edges of the volume.

To simplify the model, the whole electrode is substituted by a single particle (SPM) of solid electrode, with spherical shape and divided in spherical shells. The lithium is distributed in between the shells and it moves towards the inside or outside the external shell and among the shells as result of the applied current.

The continuum model assumes that the small volume we consider is filled up by a substance whose characteristics are the average of the characteristics of the materials present in the volume. Hence, considering the electrode material, the presence of electrolyte between the particles is neglected.

The resulting model has not poor accuracy since the considered length scale is much bigger than the particle radius. Each position  $(x, y, z)$  defines a point that could be both in the electrolyte or solid electrode material and the behavior of the material in the neighborhood of the point is known. This consideration applies to all the quantities regarding the cell.

Next step is to consider only one dimension ( $x$ ), that defines the position between the current collector of the negative electrode and that of the positive electrode. The spheres of radius  $R_s$  that model the electrode particles are centered at each  $x$  position. A “pseudo dimension” ( $r$ ) describing the lithium concentration is placed beside the  $x$  position, for this reason this model is called “pseudo-two dimensional”.

The model is still too complex for real time simulations because an infinite number of pseudo-two dimensions is present, and for each position the equations describing all the cell states need to be solved. The hint is to pass from PDEs to ordinary differential equations (ODEs), so to reduce the functions to a small order, that is still capable of returning good results.

PDEs are transformed to transfer functions, then the discrete-time realization algorithm (DRA) converts the transfer functions into state-space form, giving information about input and output, but also about the internal state of the system.

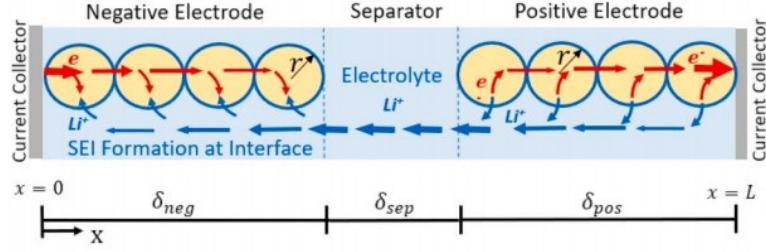


**Figure 3.7:** Schematic of the P2D electrochemical model of a cell [23].

A discrete-time formulation of the final state-space model of an LTI system is

$$x[k+1] = Ax[k] + Bu[k] \quad (3.11)$$

$$y[k] = Cx[k] + Du[k] \quad (3.12)$$

where  $x[k]$  is the state of the system and  $u[k]$  is the input, while the matrices  $A$ ,  $B$ ,  $C$  and  $D$  are obtained from the continuous-time formulation of the state-space.

It is now possible to predict the values of the reaction flux and of the potential and lithium concentration for both solid electrodes and electrolyte using the resulting reduced order model (ROM) [24]. These quantities are contained in the output vector.

$$y(t) = \begin{bmatrix} \tilde{\phi}_{s-e}(z, t) \\ j(z, t) \\ \tilde{c}_{s,e}(z, t) \\ \tilde{\phi}_s(z, t) \\ \tilde{\phi}_e(x, t) \\ \tilde{c}_e(x, t) \end{bmatrix} \quad (3.13)$$

All the values are referred to each of the four locations of figure 3.8, namely to  $x = 0$ ,  $x = L_n$ ,  $x = L_n + L_m$  and  $x = L$ , hence each component of the output vector  $y(t)$  is a vector of four elements.

A diagram that represents the variables that can be computed for the negative and positive electrodes and for the separator, is presented in figure 3.8. Electrodes potentials on both sides, namely the current collector and the separator sides of the electrodes, surface and average lithium concentrations, reaction fluxes can be evaluated for each position across the cell. Notation  $z$  in figure 3.8 represents a spatial variable within the electrodes, not the SOC as used in equation 3.1.

To further improve the model, the temperature variation can be considered. The heat generated by the cell or exchanged with the surroundings, results in a variation of the temperature of the cell. As seen in section 2.5, the temperature, in

Negative electrode ( $n$ )		Separator ( $m$ )	Positive electrode ( $p$ )	
$\phi_s(z, t)$	$\phi_e(x, t)$	$\phi_e(x, t)$	$\phi_e(x, t)$	$\phi_s(z, t)$
$c_{s,e}(z, t)$	$c_e(x, t)$	$c_e(x, t)$	$c_e(x, t)$	$c_{s,e}(z, t)$
$j_n(z, t)$				$j_n(z, t)$
$\eta(z, t)$				$\eta(z, t)$
$\phi_{s-e}(z, t)$				$\phi_{s-e}(z, t)$
$z = 0$	$z = 1$		$z = 1$	$z = 0$
$x = 0$	$x = L_n$	$x = L_n + L_m$		$x = L$

**Figure 3.8:** Variables relative to positive and negative electrodes and separator [24].

turn, affects some operational parameters or even can accelerate some degradation mechanisms.

Once the computational complexity has been reduced using ROM, still a very high quantity of data is required. It requires many characteristics of the components of the cell, as dimensions and thermal parameters of both electrodes and of the separator, and at a much smaller scale the particles dimensions, electrodes porosity and electronic conductivity, ionic conductivity and others [25, 23, 26].

### 3.3 Selection of the model

The poor availability of specific and detailed data about the cell, makes the PBM of a battery cell unachievable in the present work.

On the other hand, an ECM allows a fast prediction of the electro-thermal behavior of the modeled cell, with the need of data that can be measured [27]. Relations of the OCV to the SOC of the cell can be evaluated for different cell temperatures performing charging and discharging tests, and parameters to be used in the equivalent circuit can be extracted [28].

Generally, the quantities that are measured or estimated, are affected by sensor and process noises, introduced and accumulated in open-loop methods as the Coulomb counting. Closed-loop estimation methods are more robust in the SOC estimation, indeed they require a high computational power. An ECM can be provided with filters or observers, that are able to cancel the noise and provide automatic convergence. The most used family of dedicated algorithms are the Kalman filters.

The Kalman filter performs a prediction of the present state of the system, on the base of all past data, and an estimation by updating the predicted state with the present data, as introduced in section 5.3. The results from ECMs can be sufficiently accurate in simulating the state of the cell. In some case, such as [29],

the computed voltage is enough accurate even without any Kalman filter.

## Chapter 4

# Thermal analysis and aging mechanisms

This chapter is dedicated to the analysis of two fundamental aspects of a battery cell. They are critical issues since affecting the performance, life and safety of the battery cell. One is the influence of the temperature on the operation of the cell, dependent on the variation of the cell parameters values. The second aspect is the aging of the battery, consequence of undesired reactions or structural damage, and accelerated by certain conditions.

An overview is presented to understand the bases of the thermal model and the aging model which will be integrated with the electrical one.

### 4.1 Thermal analysis

To preserve performance, safety and life of the battery, lithium ion cells need to work in a certain temperature range, which spans from 20 °C to 40 °C [30]. Inside this interval, the behavior of a cell changes, generally without safety problems. In turn, the cell performance is dependent on the parameters that describe the cell.

As seen in section 2.5, the temperature is monitored to avoid the cells to work under unsafe conditions.

A thermal model integrated in the BMS system is necessary to predict the temperature of the core of the cell. In fact it is not possible to physically measure it. Moreover, it would have been difficult to gauge the temperature of a battery pack made up of more than 7000 cells, as in the case of Tesla cars.

When cells are being charged, one can reach a temperature a few degrees higher or lower with respect to a close cell, such as 33 °C and 27 °C. It is not a problem for the cell that it is at 33 °C, also because it is not too high. The temperature difference between the two is instead what must be avoided to reduce the risk of

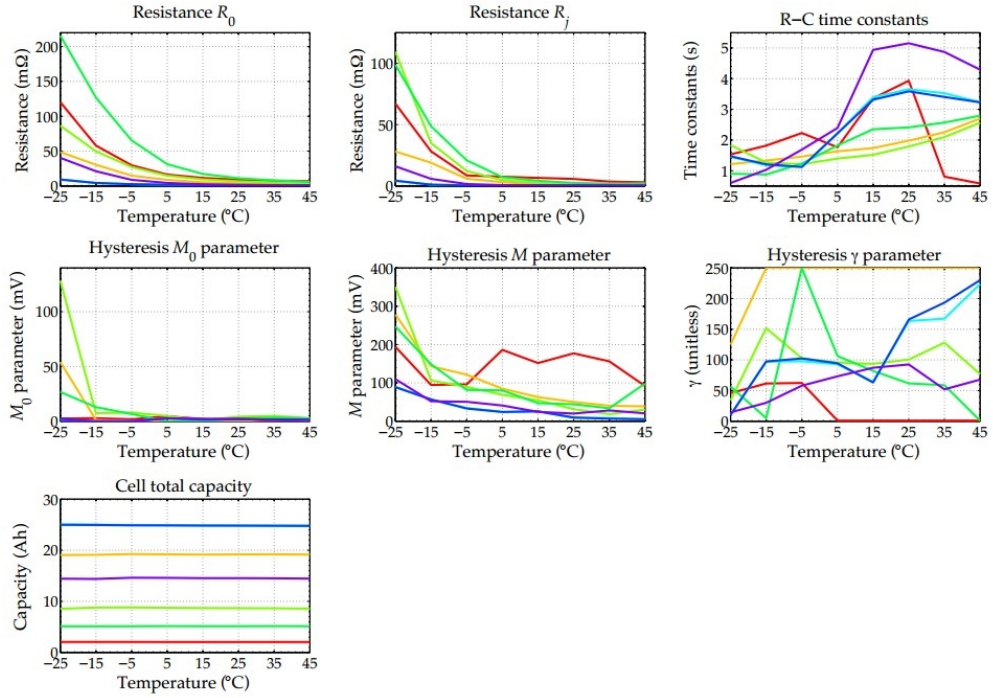


**Figure 4.1:** Variation of different cell parameters with respect to temperature [13].

localized damage [31]. Hence some temperature homogeneity should be guaranteed among the cells of the battery pack, so that cells behavior is not affected by diversity in parameters. the temperature difference should be lower than 5 °C [32].

Some studies have even analyzed the thermal behavior for different configurations of the cell, specifically of the pouch type. Different sizes for the electrodes are considered, with the result of a higher maximum temperature registered in the case of higher aspect ratio, because of the smaller volume. Also current collectors tabs location and dimension is investigated. The conclusion is a negligible influence of the tab placement on the maximum temperature and temperature distribution. On the other hand, the tab dimension has a big impact on the maximum temperature, which can be significantly reduced with increasing the tab dimension [33, 34].

The temperature gradient inside a cell is affected by thermophysical properties [35]. This leads to different aging rates across the cell. Keeping tabs on the maximum temperature and temperature heterogeneity, considering both the cases of single cell and entire battery pack, is crucial to maximize the life-cycle of the lithium ion cells [31].

### 4.1.1 Temperature control

A thermal management system is required to maintain the operating temperature inside the desired range. If the cell temperature exceeds the two limits, performances and stability can decline. Moreover, in case of extreme temperatures, thermal runaway can arise, with consequent risk of fire or explosions.

Low temperatures cause an increase in the electrolyte viscosity hence, the increase in the internal resistance of the cell [36]. This results in a decrease of the terminal voltage and so of the cell performance.

Dealing with very low temperatures, around  $-20\text{ }^{\circ}\text{C}$ , battery efficiency is highly affected [37]. Specifically, the poor battery efficiency at low temperatures is not due to a physical reduction in the capacity, but to the reduction of the rate (discharge capacity) at which charge is delivered from/to the cell, as a consequence of the parameters variations due to the change in temperature.

To control the temperature of the battery pack cells, cooling systems can be used. They are able to extract a portion of heat from the cell, by convection with air or with a cooling fluid.

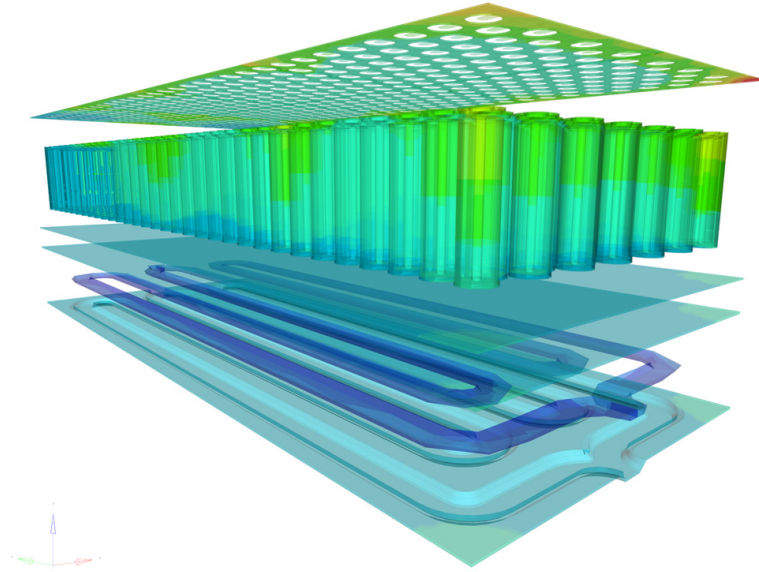


**Figure 4.2:** Example of cooling system of a battery pack [38].

When air is the fluid that is in charge of absorbing part of the heat, two methods can be used. With passive air cooling (as in Nissan Leaf), the heat generated by the cells is transmitted through conduction to the external case of the battery pack, which in turn dissipates the heat to the ambient air. A more effective solution is the active one, where the air conditioning system serves not only the passengers compartment, but also the battery pack, in order to control the cells' temperature.

When dealing with forced air systems, a “spacer” is placed in between the cells. This component, in addition to the function of keeping aligned the cells, allows the air to flow in between the glass-filled nylon material, improving the heat exchange of the cells to the air [31].

The thermal management system can be designed to heat up the battery pack in case of low temperatures, beside the cooling task.

Because of the low thermal conductivity and heat transfer efficiency of air, natural and forced air cooling systems are not so effective in dissipating the heat. This is even more crucial considering the need for fast charges, which means increasing the charging current and as consequence the thermal power developed. On the other hand, although the higher effectiveness of liquid cooling systems in controlling the cells temperature, a higher system complexity leads to higher costs [39].

#### 4.1.2 Thermal model

An electro-thermal model of the battery cell or battery pack is useful to predict the device behavior and coordinate the traction system and the thermal management system with the proper control. The model is also helpful in the design phase, to compare different battery pack configurations.

According to [27], a Thévenin circuit to model the electrical part coupled with a model to predict the thermal dynamics, provides acceptable accuracy and mathematical simplicity in simulating the battery behavior. In particular, just one RC pair is sufficient to comply with this compromise, since the transient phenomena can be well modeled because of the low C-rates that are applied on electric vehicles. For all the pieces of the circuit, the relation with the SOC and temperature is defined using look-up tables. The actual state and behavior of the system is found by interpolating the data for the working condition.

The heat generated inside a battery cell during its operation can be split into the two components: irreversible heat and reversible heat. The irreversible heat is generated by the internal resistances of the cell, known as Joule effect. The ohmic resistance and the resistances of the RC branches can be considered for the purpose [29, 40].

$$P_{th} = R_0 i^2 + \sum_{i=1}^N R_i i_{R_i}^2 \quad (4.1)$$

The current  $i$  is the battery current, that passes across the ohmic resistance  $R_0$ . The index of the summation and subscript of the resistance  $i$  indicates the different RC branches, hence  $R_i$  is the resistance of the  $i$ -th branch and  $i_{R_i}$  is the current flowing through that resistance.

The entropy effect is instead responsible for the generation of the reversible heat. As to whether the cell is charging or discharging, this quantity can be negative or positive. Moreover, it is strongly dependent on the SOC of the cell.

$$q_{rev} = iT \frac{\partial U^{avg}}{\partial T} \quad (4.2)$$

In [41] are analyzed the heat generation mechanisms, resulting in a 54 % contribution from the ohmic resistance to the total heat generation, then electrochemical reactions contribute for about 30 %. The remaining heat is developed within the polarization process.

## 4.2 Degradation factors

One big trouble with batteries is the reduction in the energy they can store and deliver. The result is the reduction of the electric vehicles range, which is itself already limited. With the progressive degradation, when some capacity conditions are reached, the battery pack needs to be substituted.

The related problems are the cost of the new battery pack and the handling of the old one. For what concerns the latter, a “second life” can be implemented, that is the use of the pack for stationary energy storage, as the case of supporting renewable energy [42]. One example is "the Battery Storage Unit" on the EUREF Campus of Berlin. Twenty battery packs from Audi e-tron are employed for storing the excess of energy produced by the photovoltaic and wind power systems, and use this as support of the grid in case of fluctuations. New processes for recycling the cells are enabling a more sustainable disposal of the devices at the end-of-life, moreover they permit the reuse of elements which are costly or ethically problematic [43].



**Figure 4.3:** Example of "second life" application of battery packs [44].

A cell reaches its end of life when the capacity reaches 80 %. Considering the various applications of batteries, the expected lifetime for reaching this condition is different. For the automotive industry the goal is set to 15 years, for smartphones 2 years, for aerospace applications at least 18 years [45].

The aging of a cell can be split in the two branches: calendar aging and cycle aging. Calendar aging is not affected by the usage of the cell, whilst it depends on the chemistry of the cell components, the SOC, the temperature and the elapsed time when no charging or discharging events occurred. The factors that affect cycle aging are the C-rate, DOD, number of cycles and the temperature at which cycles are performed. For what concerns electric vehicles, the cycle aging has a big impact on the battery pack, because of the high power involved during discharging and charging processes.

Consequences of the cell deterioration are, among the others, capacity and power fade. The capacity fade is the reduction in the quantity of energy that can be stored in the cell, due eventually to both calendar aging, to processes which can damage the cell or to undesired reactions. The same factors can be the cause of power fade, that is the reduction in the maximum power that can be delivered by a cell. Generally electric vehicles are provided with battery cells that are oversized in power, meaning that they are able to provide a power that is higher than the maximum power that can be handled by the power electronics or powertrain. As seen in section 2.5, the limitation is given by the inverter design. Thus the power fade is generally non-tangible.

### **4.2.1 Solid electrolyte interphase**

One of the main causes for capacity reduction is the SEI formation, as introduced in section 2.2. When considering the negative electrode, for instance made of lithium-titanate-oxide (LTO), the potential of graphite is very low for almost all the operational range in terms of SOC, which is good to obtain high voltage batteries. On the other hand, this electrical potential value is below the stability zone for the organic solvents used in electrolytes. The decomposition of the electrolyte solvents occurs as it comes into contact with the lithiated graphite. The process gets faster as the lithium concentration in the electrode increases, meaning that the battery charges, because the graphite potential gets lower.

When batteries are produced, they are completely discharged, so the positive electrode hosts all the lithium. As the cell is charged for the first time, a layer of SEI forms. This is called the formation process, since the SEI insulates the graphite from the solvent in the electrolyte and the layer growth is slowed down.

An undesired reaction is the consumption of lithium during the SEI film production, ending in the decrease of the capacity. The porosity of SEI still permits the lithium to intercalate and deintercalate, while the ionic conductivity decreases

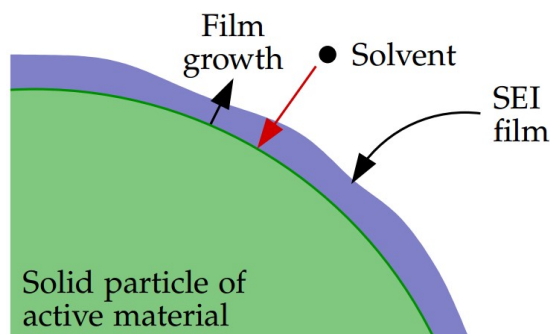


**Figure 4.4:** Diagram of SEI formation on the electrode surface [18].

and so the cell resistance increases. The result is a decrease in the capacity and in the deliverable power. Nevertheless, the pores in the SEI allow solvent to reach the graphite, so the formation of the passivating layer goes on even, if at a much lower rate.

#### 4.2.2 Secondary reactions on SEI

Some hydrofluoric acid  $HF$  can form from the reaction of water with the salt  $LiPF_6$  dissolved in the electrolyte [46]. This acid will corrode the SEI film and expose fresh graphite to the solvent, thus increasing the layer. The  $HF$  can also dissolve metals such as cobalt and manganese, causing the degradation of the electrode and the poisoning of the electrolyte [47, 48].

Another undesired event occurs when lithium deposits on the graphite anode instead of intercalating in the open structure, because of fast charging. The process is promoted when temperatures are very low, being the diffusion of lithium in the electrode, slower. This causes reduction in capacity, since part of the lithium is no longer available for passing from an electrode to the other. Moreover, the accumulation of lithium on the electrode surface, causes dendrites to build up and perforate the separator, with the effect of short circuiting the cell [49].

The intercalation and deintercalation process is responsible for the electrodes volume change. Even if expansion and contraction is limited, with cycles this process can cause the cracking of electrode particles, which makes it easier for the electrolyte solvent to reach the lithiated graphite, resulting in SEI growing.

The same passivating film formation can occur on the surface of the positive electrode, even if in a weaker way, together with the acid attack and the electrode poisoning. Inside the electrode structure, the lithium changes the molecular forces between the particles' molecules, depending if it occupies or not the site. This phase transition effect is generally reversible, but when it occurs, capacity can be reduced because lithium cannot enter a deformed site.

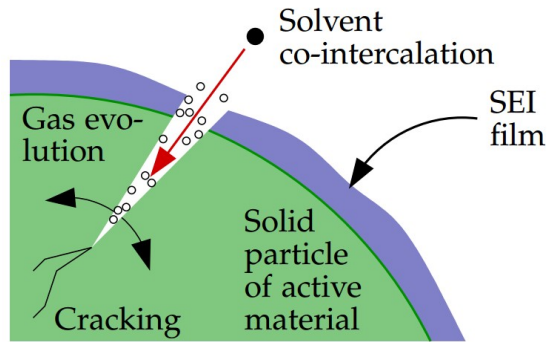


**Figure 4.5:** SEI growth because of electrode particle cracking [18].

Literature works show that high temperature has a severe effect on cell lifetime with different chemistry due to accelerated aging. The cause is the catalyzing effect of the high temperatures, which stimulates the decomposition and side reaction processes described [50]. As a loop, the series resistance increases due to aging, which results in reduction of power capability of the cell and more internal heat generation.

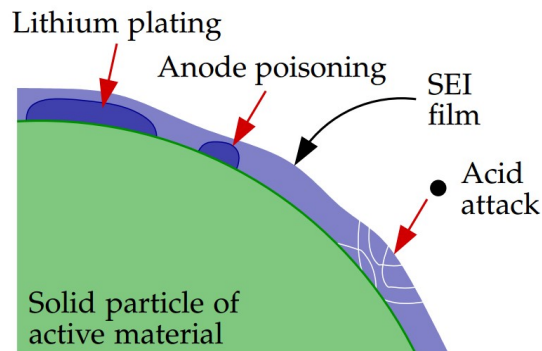


**Figure 4.6:** Secondary processes on the surface of the electrode material.

### 4.2.3 Algorithm for degradation analysis

Also in the case of aging, modeling can rely on representation of the electrochemical processes or on the description by means of equivalent circuits. The first is obviously more accurate, because it is a reproduction of the real system, whilst the latter is built performing the parameterization of the observed behavior. Data acquisition on aging phenomena requires time, furthermore it generally accounts for some of the different parameters that affect the aging, such as temperature, depth of discharge and C-rate [51].

The theory of crack propagation is applied to the electrodes material to model the cell damage due to cycling stress. In [52] a lumped parameter is used to describe the damage mechanisms. The parameter  $L$  spans from 0, when the cell has all the nominal capacity, to the value of 1 when the capacity is null. Thus, a value of the lumped damage parameter equal to 0.2 corresponds to the end of life condition of the cell. The damage parameter can be accounted for in a resistance, that is also function of the temperature and the SOC, to be put in series with the ECM [52].

The code is able to update the parameters values of the circuit model during the battery operation (online, which means in real time). It returns the increased values of internal resistance and the decrease in charge capacity. Dynamic simulations of some equivalent circuit models are able to output predictions that closely match the results of more complex electrochemical models [53, 54].

The discharging phase is practically impossible to control, since it depends on the driver requirements in terms of torque. For what concerns charging instead, a regulation on the current can be actuated. The aim of the charging algorithm is to optimize the charging time in view of the minimum aging.

# Chapter 5

## Energetic framework

### 5.1 Energetic quantities

#### 5.1.1 Pack related quantities

To obtain high performances from an electric vehicles, a high voltage is fundamental to enable high power levels, both as output to the wheels and as input when charging. The voltage that can be delivered by a cell is limited by the chemistry, but high voltages can be delivered by connecting more cells in series. The total voltage of a battery pack is:  $V_{pack} = n_s \cdot V_{cell}$

Cells connected in parallel, instead enable high currents. The total current delivered by a battery pack is:  $I_{pack} = n_p \cdot I_{cell}$

The other nominal energetic quantities relative to the battery pack can be deduced.

$$Q_{pack} = n_p \cdot Q_{cell}$$

$$E_{pack} = n_s \cdot n_p \cdot Q_{cell} \cdot V_{cell}$$

$$P_{pack} = n_s \cdot n_p \cdot I_{cell} \cdot V_{cell}$$

The number of cells connected in series  $n_s$  or in parallel  $n_p$  is determined by the following factors. The cost and size of power-electronics can be restrained by limiting the voltage, hence the number of cells connected in series. A reduction on the current, so of the number of cells connected in parallel, is beneficial for the efficiency. This reduction in losses is pursued with the aim of reducing the cost of wire, in fact a higher resistance is accepted to have a thinner section of copper wires.

To calculate the actual available energy and power, SOC, total capacity and internal resistance of all the cells of the battery pack at the present time should be known. These quantities cannot be directly measured, so they need to be estimated from the measurable quantities: pack current, cells voltages and cells temperatures.

### 5.1.2 Capacity

The total capacity  $Q$  of a cell is the quantity of charge that is extracted from a cell when it passes from a fully charged state to a fully discharged state.

Generally a cell is charged following a CC-CV profile, meaning that a constant current is delivered to the cell until the maximum voltage is reached, then the voltage is kept constant while the current decreases to an infinitesimal value. The fully charged state corresponds to the condition of maximum voltage for the cell after the CC-CV charging process, which is performed at a defined temperature and considering the OCV after a certain time has elapsed [53]. The resulting state of charge is 100 %. The discharged state corresponds to the condition of minimum voltage, where the state of charge is 0 %.

The total capacity is measured in Ah, even if its unit derived from the SI is the Coulomb, where  $1C = 1A \cdot 1s$ . The total capacity can decrease because of degradation mechanisms and aging, hence it is dependent on the SOH, beside to the C-rate and the temperature.

The discharge capacity is the quantity of charge that is removed from the cell at a constant C-rate until reaching the minimum voltage, for instance the 1C-rate discharge capacity is  $Q_{1C}$ . It is dependent on the temperature and evaluated under loading condition rather than at open-circuit.

The nominal capacity  $Q_{nom}$  is the quantity of charge the battery is designed to deliver. It is a constant value, different from the total capacity and the rated one, and specified by the manufacturer.

Finally, the residual or actual capacity of a cell is the quantity of charge the cell can deliver at present state, hence after eventual aging or damage. In any case, the usable capacity is generally lower than the nominal charge capacity, because some margin is kept to avoid damages, namely to avoid overcharge or overdischarge cases.

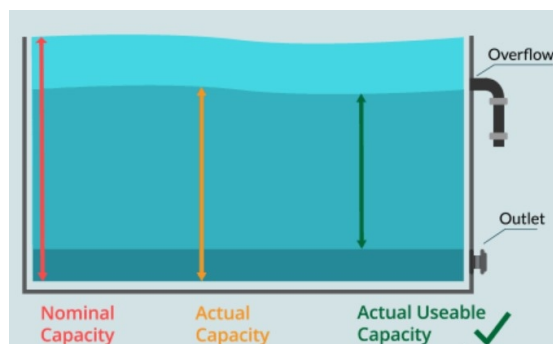


**Figure 5.1:** Visualization of the different capacity definitions. [55]

### 5.1.3 State of charge

One of the most important parameters in a battery cell is the state of charge. An accurate definition relates the SOC to the quantity of lithium that is present in the electrodes. For example, a charged cell presents a lot of Li in the negative electrode. Lithium stoichiometry at time  $k$  can be defined as the ratio between the average concentration of Li and the max concentration.

$$\theta_k = \frac{c_{s,avg,k}}{c_{s,max}} \quad (5.1)$$

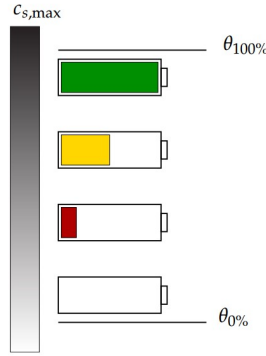


**Figure 5.2:** State of charge of the cell compared to the average lithium concentration in the negative electrode [18].

This value will be a quantity between 0 and 1 respectively for a SOC of 0 % and 100 % for the negative electrode. Hence, for the two electrodes:  $\theta_{0\%}^{neg} < \theta_{100\%}^{neg}$ ,  $\theta_{0\%}^{pos} > \theta_{100\%}^{pos}$ .

For both the positive and negative electrodes, the SOC relative to the lithium concentration is defined as follows [53].

$$z(t) = \frac{\theta_k - \theta_{0\%}}{\theta_{100\%} - \theta_{0\%}} \quad (5.2)$$

The voltage of a cell depends on the surface concentration of lithium. For this reason there is no direct correlation between voltage and SOC.

Lithium stoichiometry and average concentration in the electrodes cannot be directly measured, so SOC should be computed using the quantities that can be metered, as the voltage. Actually voltage is related to the surface concentration of lithium, while SOC depends on the average concentration of lithium in the electrodes. The quantity of lithium stored in the electrodes is directly related to the current that charges or discharges the cell, so a relationship that derives is the Coulomb Counting. It updates the SOC of the cell considering the quantity

of charge (the current involved for the considered period of time) that has been extracted from or delivered to it [53].

$$z(t) = z(t_0) - \frac{1}{Q} \int_{t_0}^t \eta(t) i(t) dt \quad (5.3)$$

It is useful to derive a discrete-time formulation of the SOC, to be used into the MATLAB model or into the BMS software.

$$z_{k+1} = z_k - \frac{\eta_k i_k \Delta t}{Q} \quad (5.4)$$

In the two relationships,  $\eta$  represents the coulombic efficiency, defined as the ratio between the total charge extracted from the cell and the total charge put into the battery. Generally its value is equal to 1 for lithium-ion battery cells [10, 53].

#### 5.1.4 Equivalent circuit model

The equivalent circuit model presented in section 3.1 can be derived in a discrete-time form, where equation 5.4 is coupled to the following two:

$$i_{R_1, k+1} = e^{\frac{-\Delta t}{R_1 C_1}} i_{R_1, k} + (1 - e^{\frac{-\Delta t}{R_1 C_1}}) i_k \quad (5.5)$$

$$v_k = OCV(z_k) - R_1 i_{R_1, k} - R_0 i_k \quad (5.6)$$

#### 5.1.5 State of health

Battery cells present a reduction of the performance when they are aged or degraded. Side reactions and damages to the electrodes structure can reduce the lithium availability, while the SEI layer can increase internal impedance and reduce charge and discharge efficiency.

To have an accurate description of the state of the cell, considering SOC, available energy and available power, the actual degradation of the cell should be known.

The quantities that describe a change in the cell performances can be used to estimate the battery health, as the residual capacity or the internal resistance.

$$SOH(t) = SOH(t_0) - \frac{\int_{t_0}^t |i(t)| dt}{N Q} \quad (5.7)$$

## 5.2 Data collection

The characterization of a battery cell and the extraction of the parameters needed to build the ESC model, require some tests under particular conditions. Each cell is connected by means of a 4-wire setup to a computer that is capable to control and acquire information about voltage, current and temperature of the cell. The device is called battery cell cycler.

As mentioned in 2.5, the Kelvin connection is used to sense the battery pack current. The two large terminals are connected to the negative wire of the battery output. The current flows through the plates, which form the calibrated resistance between the two small terminals. An ADC is connected to the small terminals to sense the voltage drop across the calibrated resistance, so the current flowing can be calculated.

$$i = \frac{v_{shunt}}{R_{shunt}} \quad (5.8)$$

The shunt resistance should be small to avoid heating through Joule effect and so power loss, hence the voltage measured is small and should be amplified.



**Figure 5.3:** Current shunt for measuring battery current.

To sense the battery temperature, a thermistor and two additional wires are required for passing the information to the cycler.

Cells must be tested at different temperatures to analyze the cell behavior and to derive the parameters relations with temperature. An environmental test chamber is used to simulate the desired ambient temperature.

The first test is executed to plot the value of the cell voltage at each point of the SOC. To have an homogeneous temperature across the cell, the cell rests for two hours at the temperature of interest, before the test starts. The fully charged cell, is then slowly depleted until the voltage reaches the minimum value defined by the manufacturer.

The output current is constant and set to a rate value of C/30. The small

current is selected to avoid effects of dynamics and to maintain an almost constant temperature, averting Joule heating.

The same procedure is applied for the charging test. The fully discharged cell is placed for two hours in the environmental chamber at the set temperature, then it is charged at a constant C/30 current rate as far as the maximum voltage is reached.

After each of the discharging and charging tests, the cell is soaked at 25 °C for two hours to check if the voltage is lower or higher than the minimum or maximum voltage, since OCV depends on temperature and because the ohmic resistance can cause a high voltage drop at extreme temperatures. Then the cell is slowly charged or discharged until reaching the maximum or minimum voltage.

To determine the coulombic efficiency, the total charged and discharged charge quantities in Ah are recorded, again for different temperatures. For instance, the coulombic efficiency at 25 °C is defined as

$$\eta(25\text{ °C}) = \frac{\text{total discharged Ah at } 25\text{ °C}}{\text{total charged Ah at } 25\text{ °C}} \quad (5.9)$$

The result, when considering different test temperatures, is a value lower than 1. In case of different lithium ion cells tested, the coulombic efficiency is generally higher than 98 %.

The parameters of the model that describe the cell response can be identified with a current pulse discharging test, by measuring the cell voltage.

As the current is applied, it ramps up in ms. The effect on the voltage is a sudden drop, due to the ohmic resistance, while a further and slower drop is due to the lithium diffusion, as identified in 2.5. The current is maintained until the voltage stabilizes, then it is removed, with the effect of an immediate voltage increase and a successive slower recovery.

At this point the value of the ohmic resistance  $R_0$  is extracted from the instantaneous voltage increase when the current pulse is removed.

$$R_0 = \left| \frac{\Delta v_0}{I_{pulse}} \right| \quad (5.10)$$

The resistance  $R_1$  of the R-C pair is instead computed from the slower voltage recovery. The considered voltage  $\Delta v_\infty$  is the difference between the total voltage recovery and  $v_0$ , and assumed to be equal to the sum of the voltage drops due to the current pulse across the two resistances. The diffusion resistance is thus computed.

$$R_1 = \left| \frac{\Delta v_\infty}{I_{pulse}} \right| - R_0 \quad (5.11)$$

Finally, the value of the capacitor  $C_1$  is estimated assuming that the voltage is stabilized after a period of 4 times the time constant of the R-C circuit, from when

the current is removed.

$$C_1 = \frac{t_{recover}}{4R_1} \quad (5.12)$$

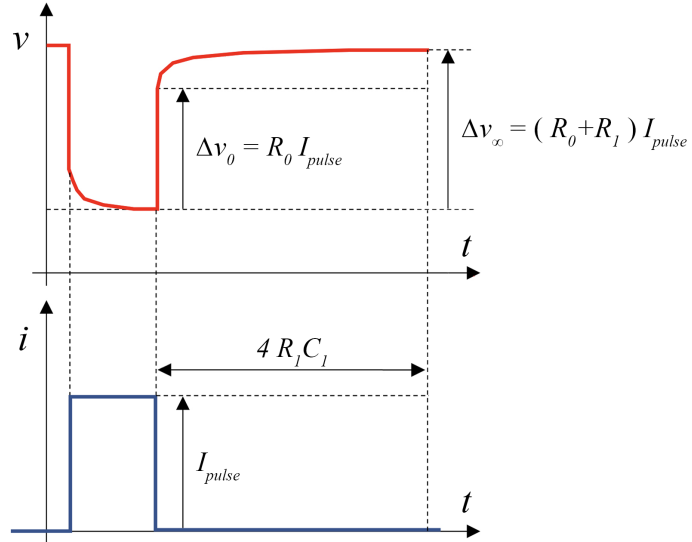


**Figure 5.4:** Current pulse and voltage response for computing cell parameters.

All the extracted values, namely the OCV profile and the electrical parameters of the cell, are stored in look-up tables, where each entry is defined for a certain SOC and temperature.

### 5.3 Estimation algorithms

A deeper analytical analysis of what is presented in section 5.1.3 returns that the cell SOC can be estimated using the measured voltage and comparing it with the OCV. This relation is accurate only if the actual voltage is metered after resting. Ohmic and diffusion voltages can be subtracted from the voltage measurement.

Anyway, the SOC is very sensitive to the change in voltage. For instance, a very small variation in voltage, in the order of tens of mV, leads to a high increase or decrease in SOC for the blue and dark green curves. Around 3.3 V, the SOC ranges from a value of about 30 % to about 70 %. The result is a very noisy relation of the SOC with respect to the voltage. Some noise can be filtered, but this action introduces a time delay in the voltage estimation.

Using the current to estimate the SOC is more intuitive. The amount of charge that flows inside or outside the battery can be calculated using the current and the

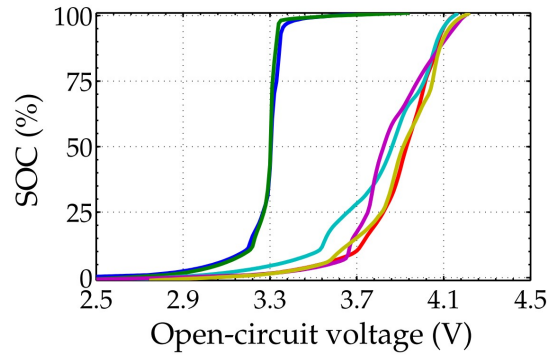


**Figure 5.5:** SOC as function of OCV for six lithium-ion chemistries.

SOC can be updated knowing its initial value and the quantity of charge normalized to the capacity of the cell.

The equation 5.4 that describes the coulomb counting for computing the SOC of the battery cell, is correct. Actually the current that is considered is not a precise value, since it is affected by many factors: noise, bias introduced by the measurement, self-discharge and current leakage make the measured value of the current different from the true value. Moreover, the values of capacity and coulombic efficiencies are also approximations, which will lead to an error in the estimation of the SOC.

The voltage and the current approaches can be blended to obtain a model-based estimation method. It presents a “true system”, where the current at the input and the voltage at the output are measured. The other branch is the model that computes the voltage using the same measured current as the true system as input.

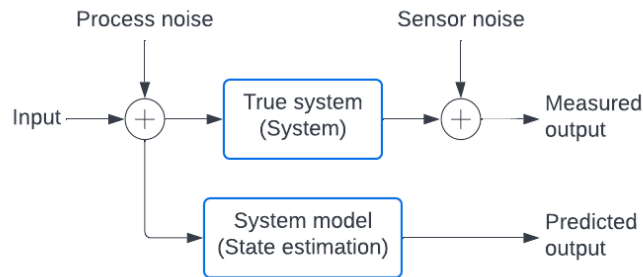


**Figure 5.6:** Diagram of the model-based estimation approach.

The system features diffusion currents and hysteresis voltages that must be estimated. Moreover there are the uncertainties introduced by process and sensor

noises. The first leads to a change in the state of the cell since the measured current might differ from the true value, the latter gives a non-fully trustable measured value. For this reason a comparison of the outputs of the two branches is performed. The difference of the two voltages can be used as feedback to update the model and consequently to improve the goodness of the state estimation.

Again, the voltage error is not truthful because of the errors in the measurement and in the estimation, due to the model that is not a perfect description of the real system.

Sequential probabilistic inference (SPI) can be used to estimate the state of a system for which some observed values are noisy or incomplete.

$$x_k = f(x_{k-1}, u_{k-1}, w_{k-1}) \quad (5.13)$$

$$y_k = h(x_k, u_k, v_k) \quad (5.14)$$

The system is identified through a state-space description.  $x_k$  indicates the present state and is a function of the past state and input and is influenced by the past process noise  $w_k$ . The output  $y_k$  is a function of present state and input and of the sensor noise  $v_k$ , so it is not the true voltage since it is affected by a certain noise. Both noise signals are random and unmeasurable.  $u_k$  is the cell current that is measured and used as input for both branches of the model-based estimation.

Since the actual state is predicted using information about the past, the solution is defined as “sequential”. The term “probabilistic” is related to the process and sensor noises, which are random signals.

In figure 5.7 the system evolution with discrete time  $k$  of the state and output is illustrated. The state is not measurable, but it is possible to pass from the state  $x_{k-1}$  to the state  $x_k$  using the conditional probability density function  $f_{X|X}(x_k|x_{k-1})$ , which accounts also for the process noise uncertainty. The system output  $y_k$  is instead observable, so it can be used for state estimation. The sensor noise uncertainty is considered in the conditional probability density function  $f_{Y|X}(y_k|x_k)$ . The uncertainties lead to an error in the estimation of the state. Hence, beside the estimation, it is necessary to know a certain interval of values that the state can assume.

Being noise a random quantity, even repeating the same test, the observed quantities are different because of noise influence. The random variables are the quantities that cannot be precisely predicted, but for which the probability to assume a certain value is known. The function that describes the likelihood of a measurement  $X$  to assume the value  $x$  is the probability density function (pdf)  $f_X(x)$ .

The Gaussian distribution is the most important probability density function, also called normal distribution. For a pdf, some quantities can be defined, which

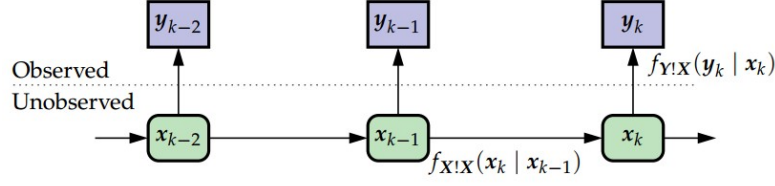


**Figure 5.7:** Diagram of the sequential probabilistic inference concept.

are defined as “moments” of a statistical distribution. The first moment is the mean of the distribution, which indicates the center of gravity of the function. The mean value or expected value of the random variable  $X$  is given by

$$\bar{x} = \mathbb{E} = \int_{-\infty}^{\infty} x f_X(x) dx \quad (5.15)$$

The difference between the random variable and the mean can be squared, and the expected value of this quantity is defined as variance.

$$\text{var}(X) = \mathbb{E}[(X - \bar{x})^2] = \mathbb{E}[X^2] - \bar{x}^2 \quad (5.16)$$

The standard deviation of a random variable  $X$  is simply  $\sigma_X = \sqrt{\text{var}(X)}$ . Generally a pdf is concentrated around the mean value and the variance describes how the function is distributed around the mean. The lower the variance, the smaller the interval in which the probability is higher. The variance is the second moment of a distribution.

Finally, the Gaussian pdf of a random variable  $X$  that has mean  $\bar{x}$  and variance  $\sigma_X^2$  is given by

$$f_X(x) = \frac{1}{\sqrt{2\pi}\sigma_X} \exp\left(-\frac{(x - \bar{x})^2}{2\sigma_X^2}\right) \quad (5.17)$$

which can be written in a more compact notation as  $X \sim N(\bar{x}, \sigma_X^2)$ . The empirical rule for a Gaussian distribution states that 99.7 % of the observed data lies in the interval  $\pm 3\sigma_X^2$  around the mean.

When dealing with more random variables, these objects can be collected in a vector. Each entry  $X_i$  of the random vector is related to a probable value  $x_i$  of the sample vector by means of the joint pdf. Also for the random vector, a mean or expected value can be computed.

$$\bar{x} = \mathbb{E}[X] = \int_{-\infty}^{\infty} \int_{-\infty}^{\infty} \dots \int_{-\infty}^{\infty} x f_X(x) dx_1 dx_2 \dots dx_n \quad (5.18)$$

The outer product of the vector is performed for computing the square correlation matrix

$$\Sigma_X = \mathbb{E}[X X^T] \quad (5.19)$$

The square covariance matrix is

$$\Sigma_{\tilde{X}} = \mathbb{E}[\tilde{X}\tilde{X}^T] \quad (5.20)$$

being  $\tilde{X} = X - \bar{x}$ . The variances  $(\Sigma_{\tilde{X}})_{ii} = \sigma_{\tilde{X}_i}^2$  of the scalar random variables are placed on the diagonal. The other entries are proportional to the product of the standard deviations of the random variables  $X_i$  and  $X_j$

$$(\Sigma_{\tilde{X}})_{ij} = \rho_{ij}\sigma_{X_i}\sigma_{X_j} = (\Sigma_{\tilde{X}})_{ji} \quad (5.21)$$

The pdf of a random vector can be written as

$$f_X(x) = \frac{1}{\sqrt{(2\pi)^n |\Sigma_{\tilde{X}}|}} \exp\left(-\frac{1}{2}(x - \bar{x})^T \Sigma_{\tilde{X}}^{-1} (x - \bar{x})\right) \quad (5.22)$$

The random variables collected in a random vector can be defined as independent if and only if the joint pdf of the vector is equal to the product of the marginal pdfs of each random variable. Moreover, two random variables  $X_i$  and  $X_j$  of a random vector are uncorrelated if their standard deviations are finite and, for  $i \neq j$ , the covariance is null. This means that  $\rho_{ij} = 0$ , and if all the random variables are uncorrelated, the square covariance matrix is diagonal. The conditional pdf returns the probability that  $X_1 = x_1$  when  $X_2 = x_2$ .

$$f_{X_1|X_2}(x_1|x_2) = \frac{f_X(x_1, x_2)}{f_{X_2}(x_2)} \quad (5.23)$$

Finally a conditional expectation  $\mathbb{E}[X|Y = y]$  returns the expected value for the random vector  $X$ , knowing that  $Y = y$ .

Given an introduction on probabilistic quantities, the steps for implementing the solution of a Gaussian SPI is presented. This is the basis for the different types of Kalman filters. The six steps can be grouped in two processes, which are the prediction and the correction of the state.

The three steps of the prediction process are:

- 1a. time update of the state-prediction, based on measurements taken at the previous time step,
- 1b. error-covariance time update, where the state-estimate error covariance matrix is predicted using past information,
- 1c. prediction of the system output, knowing last time step output and measuring the actual input.

The correction process includes the following three steps:

- 2a. estimator gain matrix computation,
- 2b. update of the state-estimate measurement, which is revising the prediction through a comparison with the actual measurement of the output,
- 2c. update of the error-covariance measurement.

The point of using a Kalman filter is to minimize the error in the estimation of the state, or more precisely to find the minimum mean square error (MMSE). The illustrated steps are valid for a linear system that presents white and Gaussian noises. Generally the cell model is nonlinear, for this reason some methods to approximate the system need to be applied. The three main strategies for coping with nonlinearities are:

- the extended Kalman filter (EKF), which linearize the system around the current state estimate by truncating to the first order the Taylor series expansion at each time step,
- the sigma-point (SPKF) or unscented (UKF) Kalman filter alleviates the errors introduced by EKF in the estimation because of the approximation. The idea is to linearize the distribution of the state random variable, rather than linearizing all the system,
- the particle filters are used when problems do not present Gaussian distribution or feature a multimodal distribution. These filters are based on Monte Carlo simulation, where a simpler distribution is substituted to the real one, then some samples (called particles) of past distribution are weighted and summed to obtain a distribution similar to the real one. Obviously this method is the most accurate.

# Chapter 6

## Model definition

In this chapter, the model is presented conceptually and in its construction and operation. Three sub-models are studied and implemented for describing the mechanisms of chapters 3 and 4.

The battery is modeled by means of an equivalent circuit model, that simulates the electric behavior of the cells. Depending on the current that is flowing out of the cell or into it, the voltage and the SOC change.

The temperature variation and its influence on the cell parameters are presented in the thermal model. The process is again governed by the current that produces some heat because flowing through the ohmic and the diffusion resistances.

The model that describes the loss of capacity and consequent reduction of the SOH is also integrated in the system. The temperature of the cell and the total charge quantity released by or introduced in the battery are critical issues regarding the life of the device.

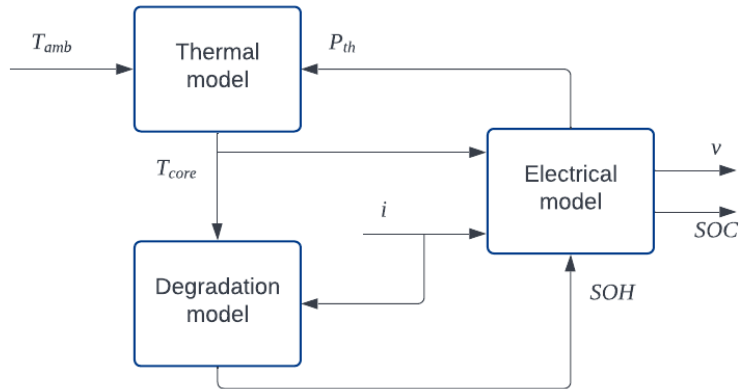


**Figure 6.1:** Diagram of the interactions between thermal, degradation and electrical models.

## 6.1 Heat generation and temperature variation

The first block of the flowchart is the thermal model. The idea comes from the fact that the cell parameters vary according to the temperature. As seen in section 4.1, the current that flows through a resistance causes power dissipation in the form of heat. This condition is verified through the ohmic resistance and the resistances of the RC branches that describe the lithium diffusion. The first step is to compute the power that is dissipated by the cell as “Joule effect”. Starting from equation 4.1, the thermal power is evaluated considering just one RC branch for the electrical model.

According to different studies [56, 57, 58, 59] the entropic heat is very small if compared to the ohmic heat generation, particularly in case of high currents. The result is that the contribution from reversible heat is neglected.

$$P_{th} = R_0 i^2 + R_1 i_{R_1}^2 \quad (6.1)$$

At this point the thermal model is developed, with the thermal power as input. The basis of the thermal model is [60], where a formulation for the energy balance of battery systems is presented.

The dynamics of heat transfer are analyzed, considering different processes: chemical reactions, phase changes, variation in the heat capacity and heat transfer to the surroundings. For the purpose of this work and the data availability, the

model will consider the heat transfer dynamics across a cylindrical cell as presented in [61].

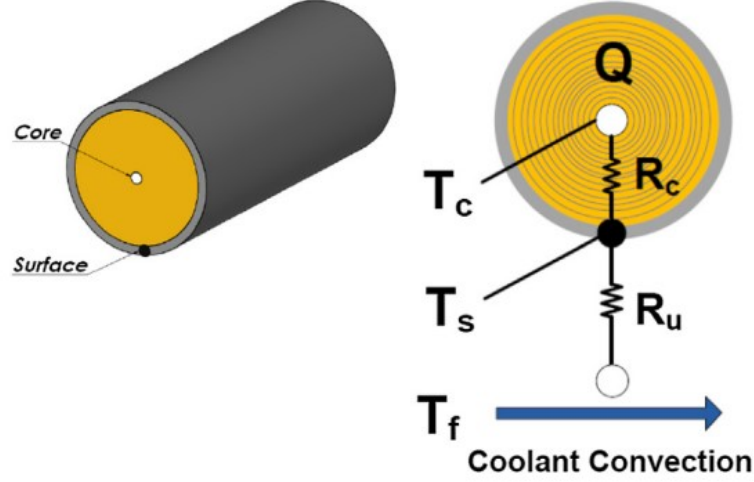


**Figure 6.2:** Diagram of the thermal model of the battery cell [61].

The model accounts for the temperatures of the core and of the surface of the cell. The heat dissipated because of the fluid that act as coolant, namely air or liquid coolant, on the surface of the cell is also considered. The points are connected by resistances, which are the heat conduction resistance  $R_c$  of the cell material, in between the points of the core and the surface, and the heat convection resistance  $R_u$  relative to the air or the liquid cooling fluid.

At this point, the formulation of the heat transfer can be applied.

$$\frac{dT_{core}(t)}{dt} = \frac{T_{cell}(t) - T_{core}(t)}{R_c C_c} + \frac{P_{th}(t)}{C_c} \quad (6.2)$$

$$\frac{dT_{cell}(t)}{dt} = \frac{T_{amb}(t) - T_{cell}(t)}{R_u C_s} - \frac{T_{cell}(t) - T_{core}(t)}{R_c C_s} \quad (6.3)$$

The two components  $C_c$  and  $C_s$  are the core heat capacity and the surface heat capacity.

The thermal model is implemented using the MATLAB Function block of Simulink. The given input to the model is the thermal power simply calculated as in equation 6.1, together with the initial conditions of the temperatures, namely the cell core, the cell surface and the fluid temperatures. The latter is supposed to be constant as in [60].

The system of the two equations 6.2 and 6.3 describing the thermal dynamics is implemented in the MATLAB Function as in figure 6.3. The time is now considered

as discretized quantity  $k$  as for the SOC. The output are the derivatives of the core and the surface temperatures of the cell, hence an integrator block is placed, with the initial condition specified. Since a "for cycle" is used for the simulation of the cell behavior with time, the initial conditions are updated for every iteration with the temperatures state of the previous cycle. The outcome of the two "Integrator" blocks are sent as input to the MATLAB Function as actual temperature state of the cell.

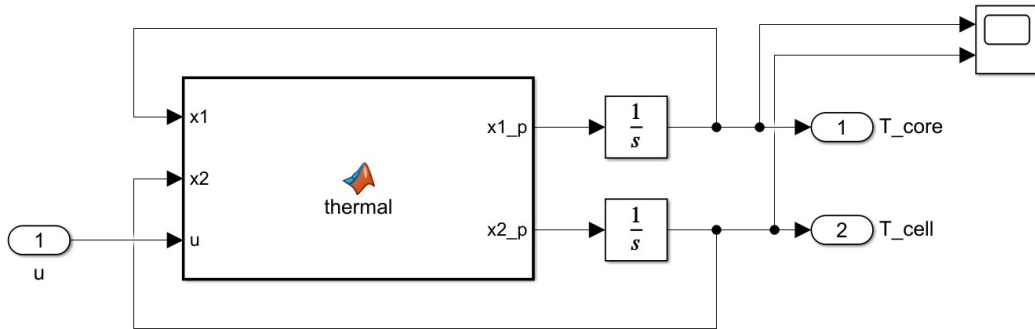


**Figure 6.3:** MATLAB Function implemented on Simulink to model temperature evolution.

To analyze different cells or different working conditions, heat conduction and convection resistances, cell and fluid capacitances and all the starting temperatures can be changed into the MATLAB Function script.

At this point the temperature behavior as current is provided to the cell with time is known. The results are feed back to the workspace and extracted.

As seen in 4.1, the cell parameters are dependent on the temperature, hence also the cell behavior is affected by the heat generation and dissipation dynamics. The temperature value is now used to extract from the database all the required data, for the specific cell, at the considered temperature and at the present SOC.

The parameters  $R_0$ ,  $R_1$  and  $C_1$  are not measurable, since they are not physically present in the real cell. Instead they can be used all together to represent some physical properties or processes as the voltage drop due to the ohmic resistance or the lithium diffusion into the electrodes. For example, OCV varies according to the SOC but also with the temperature. Also the capacity and internal resistance are affected by T. Hence, all the parameters that describe the cell behavior in the equivalent circuit model, are updated with the temperaure, such as the ohmic resistance in figures 7.5 and 7.9. The C-rate is updated in case the current changes.

## 6.2 Capacity loss

Next step is to consider the aging model. It has been shown in 4.2, that the factors which affect the degradation of a cell are

- the time, for calendar aging or cycling time,
- the temperature, that promotes some reactions or causes the reduction of capacity,
- the depth of discharge and C-rate, which are indexes of the stress the cell is subjected to.

To obtain data about aging, cells are tested at different C-rates and temperatures, for different depths of discharge. An example is [62], where cells are cycled with a depth of discharge of 90, 80, 50, 20 and 10 %, for C-rates of 1/2, 2, 6, 10, all under temperature conditions of -30, 0, 15, 25, 45 and 60 °C.

Some tests stopped soon because of the high loss of capacity during cycling, or even failed at the first test. The cells had poor performances when testing at extreme conditions, as excessively high or low temperatures, or high current intensity.

A general equation that fits the registered data, considering the different factors, is

$$\Delta Q = B e^{\frac{-E_a}{RT}} t^z \quad (6.4)$$

where  $\Delta Q$  is the capacity loss,  $B$  is pre-exponential factor,  $E_a$  activation energy,  $R$  gas constant,  $T$  temperature of the core of the cell,  $t$  the time and  $z$  power law factor [63]. Those parameters are evaluated for the different C-rates at which cells have been tested.

In the MATLAB code for the aging model all the values are interpolated for the actual current intensity, using `interp1` function.

A better description of the cell usage can be formulated using the total quantity of charge delivered by the cell in its cycling history, instead of time in equation 6.4. This quantity is the total throughput (Ah) and depends on the number of cycles  $N$ , the depth of discharge and the total capacity.

$$A_{thr} = N \times DOD \times Q \quad (6.5)$$

The result is

$$\Delta Q = B e^{\frac{-E_a}{RT}} A_{thr}^z \quad (6.6)$$

Because of the range requirements from an electric vehicle, the maximum capacity loss acceptable for a battery pack is 20 % as reported in section 4.2.

Equation 6.6 can be used to extract the total throughput that a cell can handle under the considered conditions of temperature and current intensity.

$$A_{thr} = \left( \frac{\Delta Q}{B e^{-\frac{E_a}{RT}}} \right)^{\frac{1}{z}} \quad (6.7)$$

Knowing the cell capacity and depth of discharge of the cycles and from equation 6.5, the total number of cycle correspondent to the computed charge quantity can be evaluated:

$$N = \frac{A_{thr}}{Q} \quad (6.8)$$

The SOH is derived from the definition using equation 5.7.

### 6.3 Electrical model

The outcome of the thermal model, that is the temperature variation during cell usage, is used to update the parameters of the cell.

Moreover, the temperature is the input of the aging model, together with the current intensity.

The thermal model and aging model are recalled at each iteration of the simulation time, and they are able to update the temperature and the SOH of the cell.

Once all the models are joined together, some test can be performed to evaluate the goodness of the model.

# Chapter 7

## Results

The outcome of the model are presented in this chapter. Different current intensities are selected as input for the tests, in order to evaluate the temperature increase and the influence on the degradation.

Since a real cell to be tested is not available, neither are the test equipment, the model output is compared to the literature and studies available.

Datasheet relative to some cells have been downloaded from "University of Colorado Colorado Springs" website<sup>1</sup>.

### 7.1 Dataset used for the model

The file contains data relative to six different cells, which are not specified. Functions are provided to extract the required data from the Excel files, as the OCV relative to each point of the SOC, the value of the ohmic resistance and to the time constant. The latter is used to compute the resistance of the RC branch that describes the lithium diffusion in the electrode. Other data included in the datasheet are the capacity of the cell and the coulombic efficiency. All the parameters are given for different temperature conditions, since their value change according to the temperature. The set of temperature is -25, -15, -5, 5, 15, 25, 35 and 45 °C.

Finally, all the information are put in a MATLAB structure called "model", to be available in the workspace during simulations.

Among the six cell datasheets, the selected one is named "A123". The choice comes from the comparison of the available data with the information contained in some studies. The cited articles present studies on a 26650 cylindrical model of battery cell, from A123 manufacturer. The cell features a capacity of 2.3 Ah. The value of the OCV of the cell from the datasheet are plotted together with the

---

<sup>1</sup><http://mocha-java.uccs.edu/BMS1/CH02/ESCtoolbox.zip>

SOC. The result is compared with the studies. The same is done for the internal ohmic resistance, whose values are plotted in relation to the SOC and for different temperatures. The code for extracting and plotting the data is reported in appendix A.1.

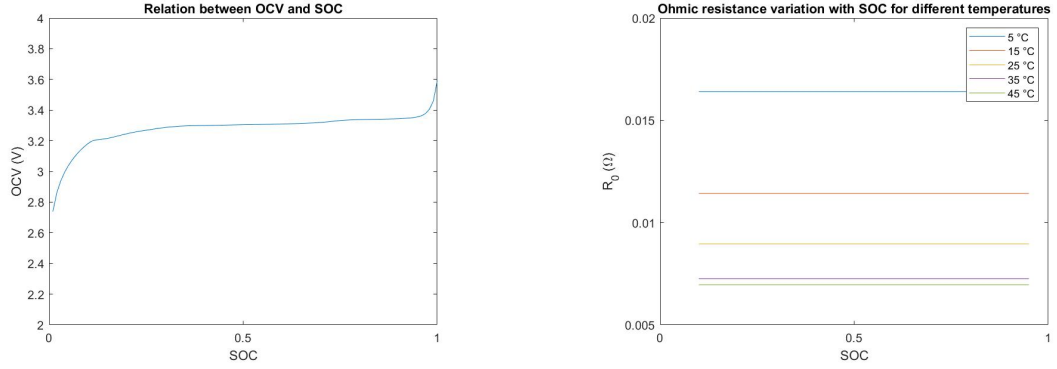


**Figure 7.1:** OCV and ohmic resistance variations from online datasheet.

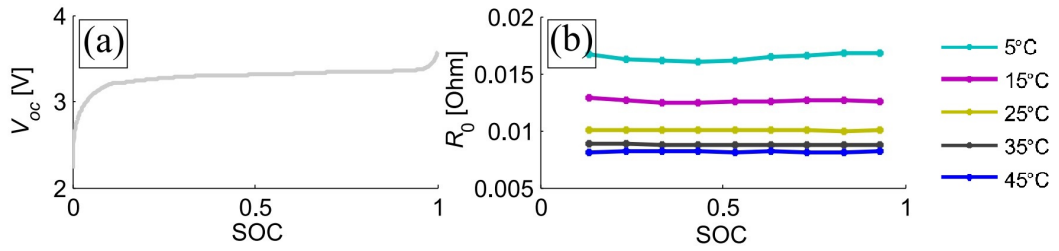


**Figure 7.2:** OCV and ohmic resistance variations from online articles.

The relation of OCV presents an identical profile, with the The other parameters of the electrical model, are not compared since the ECM includes a single RC branch for simulating lithium diffusion, while in [64] two RC branches are used. Since the time constant is just one in the ECM and two in the article, the result of their relations with temperature and SOC are different.

Next step is to find data relative to the thermal characteristics of the cell. Actually the datasheet contained only electrical parameters.

To apply the thermal model seen in 4.1.2, resistances and heat capacities relative to the materials of the cell or to the fluid that is in contact with the surface of the cell are needed to solve the heat transfer equations 6.3 and 6.2.

The values of heat conduction and convection resistances  $R_c$  and  $R_u$  and of core and surface heat capacities  $C_c$  and  $C_s$  are from [65] since relative to the cell from A123 manufacturer and with similar characteristics to the cell of the used database. The values of the presented terms are reported in table 7.1.

$R_c$	$R_u$	$C_c$	$C_s$
$35.5 \frac{K}{W}$	$2.8 \frac{K}{W}$	$50.0 \frac{J}{K}$	$2.8 \frac{J}{K}$

**Table 7.1:** A123 cell thermal parameters

The results of the temperature evolution can be seen in for instance in figures 7.4 and 7.8.

The aging model is the next block implemented. Also data relative to the cycling of the cell, durability and stress tests, are not provided in the datasheets. The article [62] has conducted some tests on an A123 cell model. Cyclic tests for different current intensities and depth of discharge and for different temperatures returned data about the degradation of the cell and the SOH variation.

The fitting of the data of the analysis gives the parameters that are necessary for the aging model presented in 6.2, so to compute the capacity loss, with given temperature and current intensity. The latter is responsible for the variation of the parameters of the aging model, while the temperature affects the activation energy.

The needed values to be used in equations 6.6 are the pre-exponential factor, the activation energy and the power law factor.

Values relative to that cell are reported in table 7.2.

C-rate	B	$E_a$	z
$\frac{1}{2}$	30330	$31500 \frac{J}{mol}$	0.552
2	19300	$31000 \frac{J}{mol}$	0.554
6	12000	$29500 \frac{J}{mol}$	0.56
10	11500	$28000 \frac{J}{mol}$	0.56

**Table 7.2:** Parameters for computing the capacity loss for different C-rates

At this point, all the information needed to run the complete thermal-aging-electrical model are collected.

## 7.2 Outcomes of the simulations

Some tests are here presented.

The tests are conducted on a single cell for a first analysis of the outcomes of the model.

The model is fed with the mentioned data and the quantities that can be selected for each specific testing conditions are the current intensity, the ambient

temperature and resting temperature of the cell, the initial SOC and the final one, that is the point at which the cell stops charging.

The testing conditions are set as input in the script A.2, and selected in order to compare the results with the analyses performed by articles [64, 65].

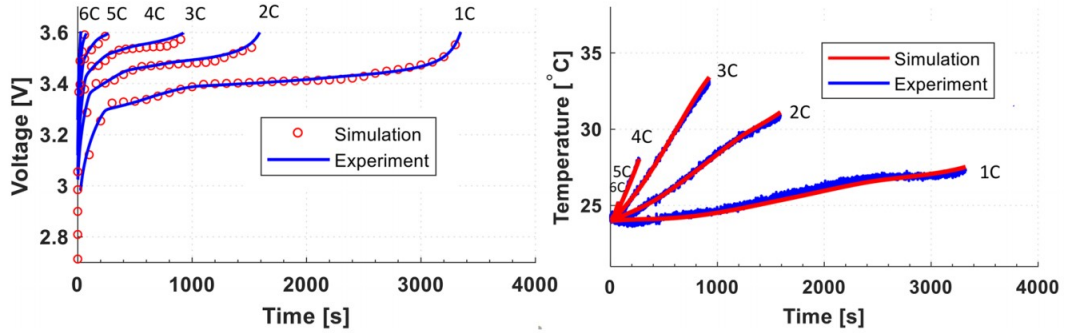


**Figure 7.3:** Voltage and temperature evolution during charging at different C-rates [65].

### 7.2.1 2C at 25 °C

The first test is conducted with a C-rate of 2, meaning that the cell is charged with a current of 2.3 A. The temperature under which the test is simulated is 25 °C. The boundaries that are set for the SOC are 0 % for the starting point and 100 % for the moment at which the charging stops, so a full charging session.

A charging time of 30 minutes is selected for the simulation.

The first plot represents the temperature increase of the cell core during charging. As clearly visible, the heat generation leads to a temperature increase of about 5 °C.

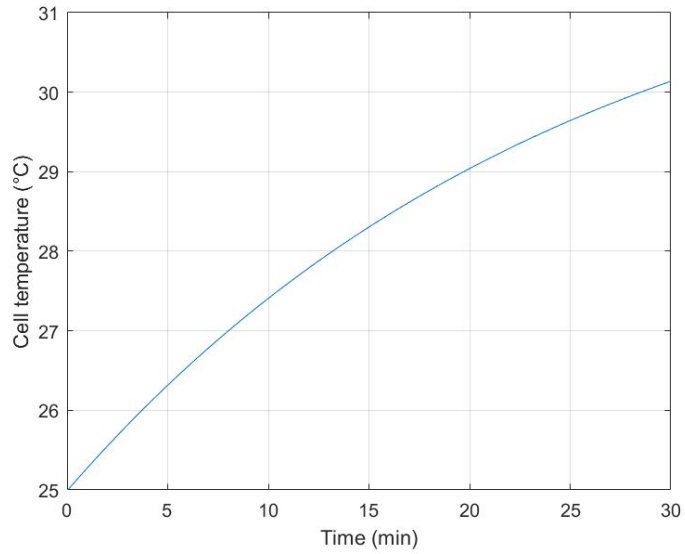


**Figure 7.4:** Temperature variation during 2C charging simulation at 25 °C.

The little temperature variation leads to a small variation in the internal resistance. The total decrease is in the order of  $10^{-3}m\Omega$  across the charging process.

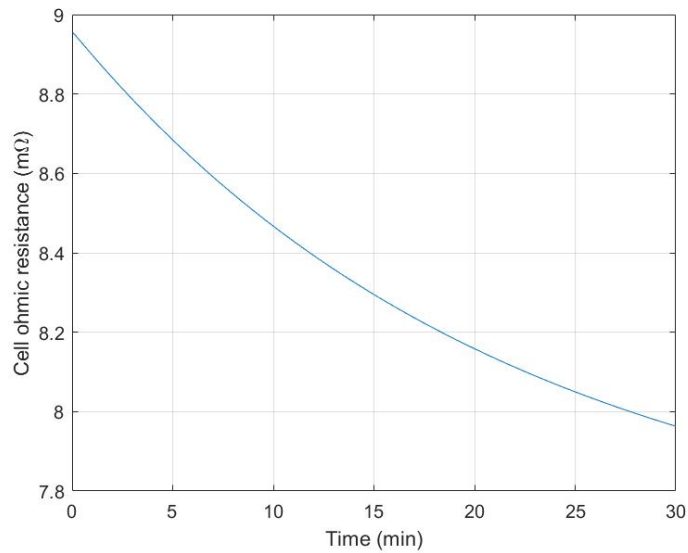


**Figure 7.5:** Ohmic resistance variation during 2C charging simulation at 25 °C.

The set simulation time of 1800 seconds is perfectly coincident with the charging

time. Indeed after 30 minutes the cell has reached 100 % of SOC, when the cell voltage reaches the maximum value of 3.6 V. Both the temperature evolution and voltage behavior during charging match the plots of figure 7.3. In the test case, the fully charged condition is reached at 1800 s, while in [65] it takes more or less 200 seconds less. The reached temperature is in both cases slightly higher than 30 °C.

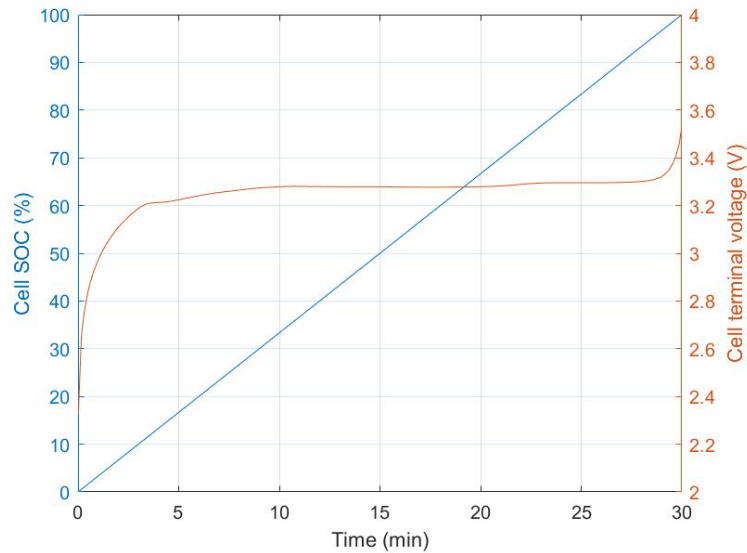


**Figure 7.6:** SOC and cell terminal voltage variation during 2C charging simulation at 25 °C.

The gentle charging conditions, namely low current intensity and consequent not high increase in core temperature, result in a negligible capacity loss and consequent reduction in SOH.

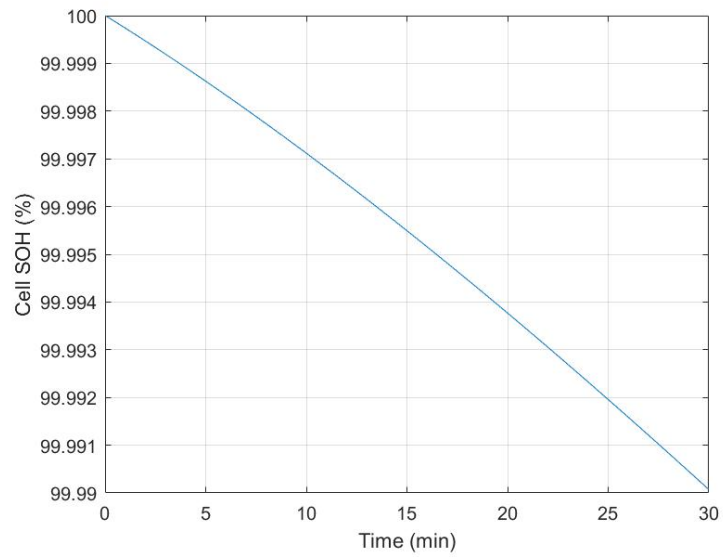


**Figure 7.7:** SOH variation during 2C charging simulation at 25 °C.

### 7.2.2 3C at 25 °C

A test is conducted with a C-rate of 3, again at 25 °C and with a simulation charging time of 1200 seconds.

The temperature increase results higher than in the case of 2C current intensity, because of the higher quantity of heat developed.

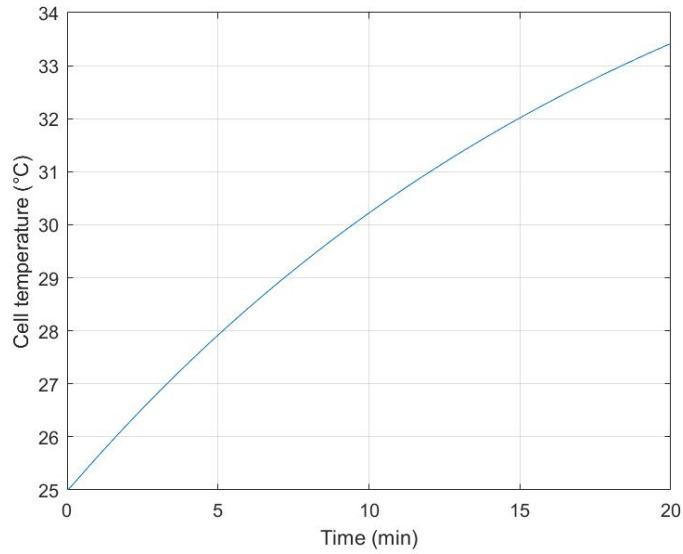


**Figure 7.8:** Temperature variation during 3C charging simulation at 25 °C.

The ohmic resistance decreases at a higher rate as effect of the increase in temperature. The decrease across the charging process is in the order of  $1.4\text{ m}\Omega$ .

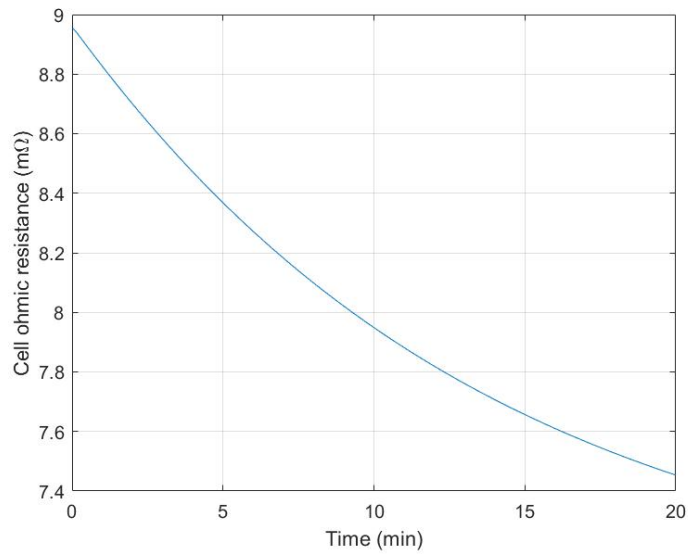


**Figure 7.9:** Ohmic resistance variation during 3C charging simulation at 25 °C.

Again, the set simulation time of 20 minutes resulted equal to the charging time. After 1200 seconds the cell passes from 0 to 100 % of charge.

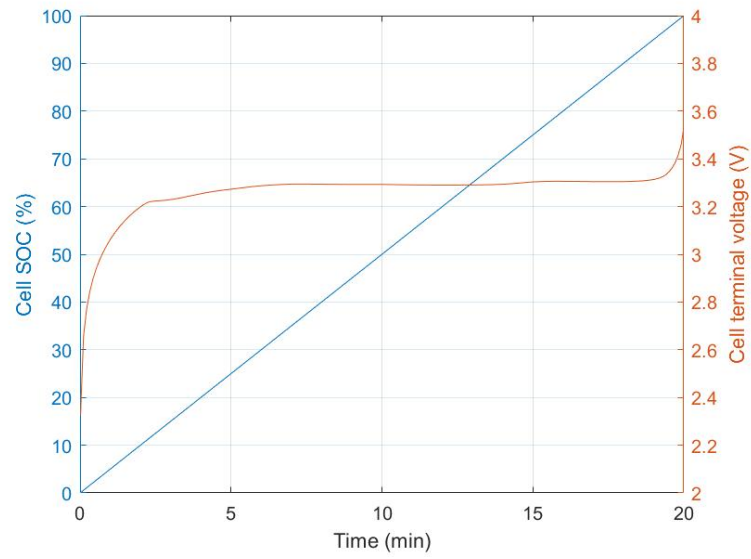


**Figure 7.10:** SOC and terminal voltage variation during 3C charging simulation at 25 °C.

A slightly higher capacity loss is registered because of the higher temperature conditions and cell stress due to the higher charging rate.

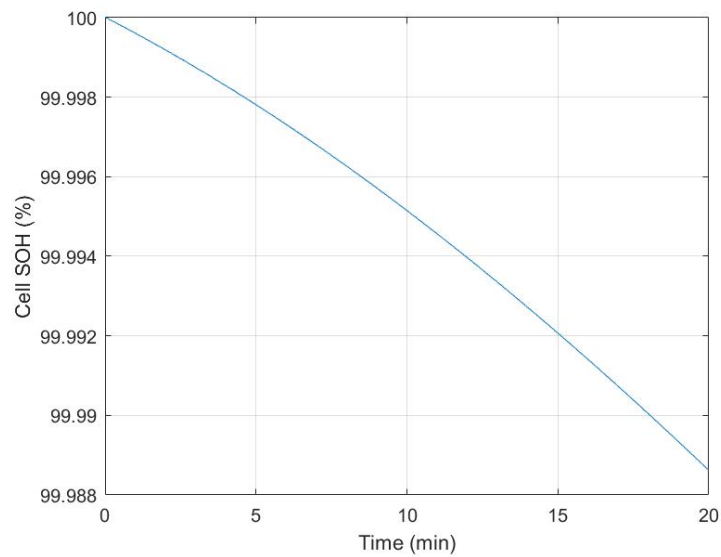


**Figure 7.11:** SOH variation during 3C charging simulation at 25 °C.

### 7.2.3 5C at 25 °C

This test is instead compared to the one reported in figure 7.12, considering the 5C current intensity.

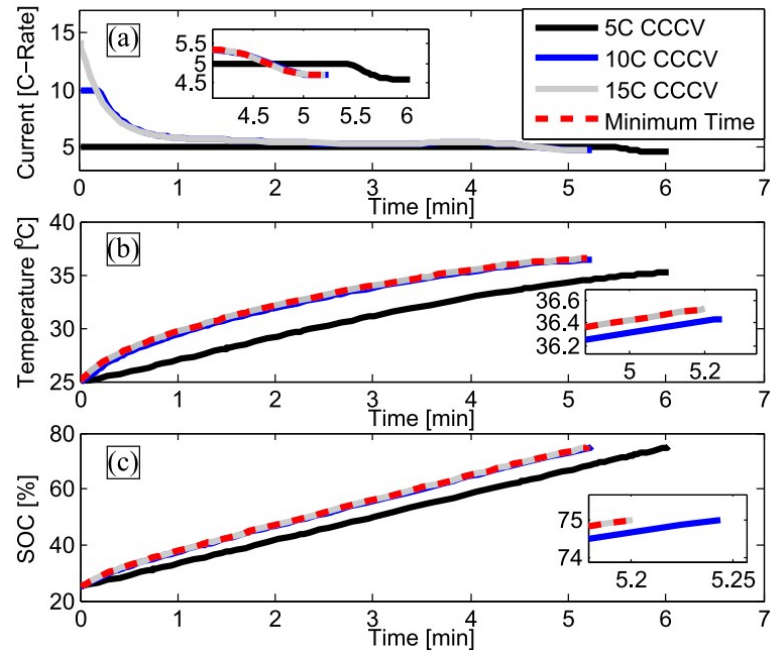


**Figure 7.12:** Test conducted at different C-rate with resulting temperature and SOC increase [64].

The results of the thermal-aging-electrical model match also this different article. A final temperature very close to 35 °C a SOC of 75 % that is reached starting from 25 % after 6 minutes are common results for both the analyses.

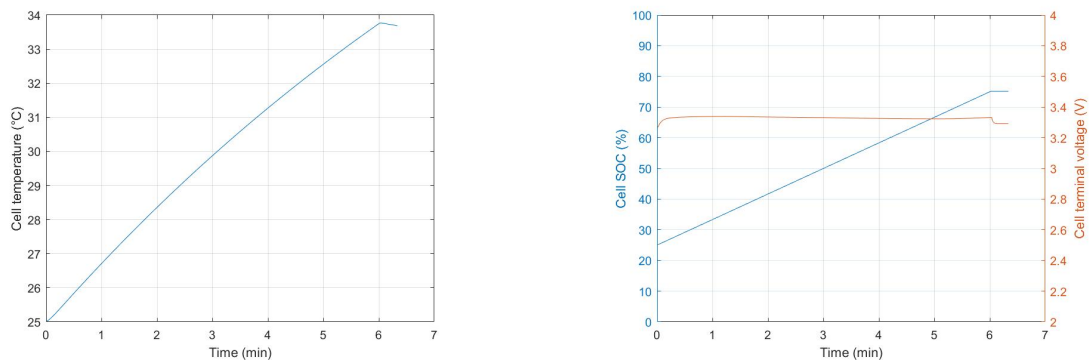


**Figure 7.13:** Temperature, SOC and voltage evolution for a test at 5C.

### 7.2.4 Test replicated from article

Last test conducted on a single cell is replicated from article [64]. It represents a strategy of minimum charging time. The current evolution is roughly reproduced using two straight lines with different inclinations.

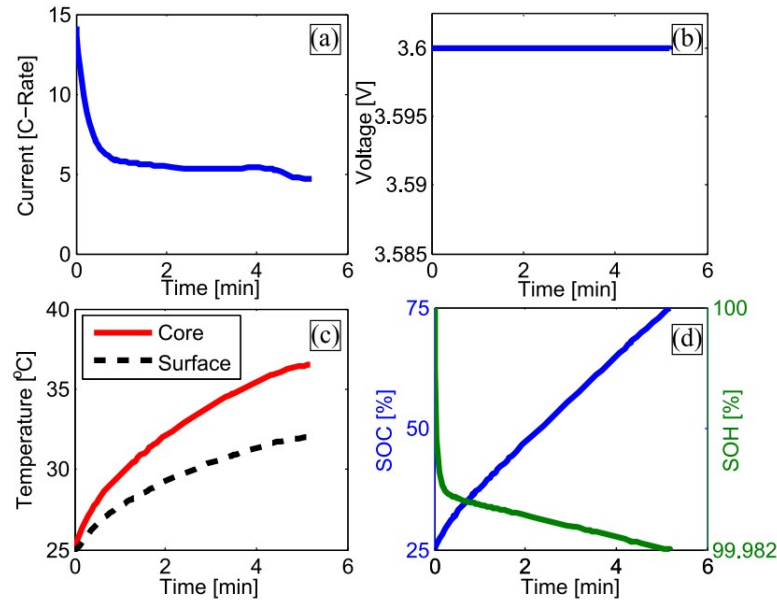


**Figure 7.14:** Test for the minimum charging time [64].

The results from the model perfectly match the outcome of the article. Both plots show a temperature slightly higher than 35 °C at the end of the test, a SOC of 75 % after 5 minutes of charging and a degradation of 99.982 % of residual SOH for the article, while the model returns a value of 99.984 %.

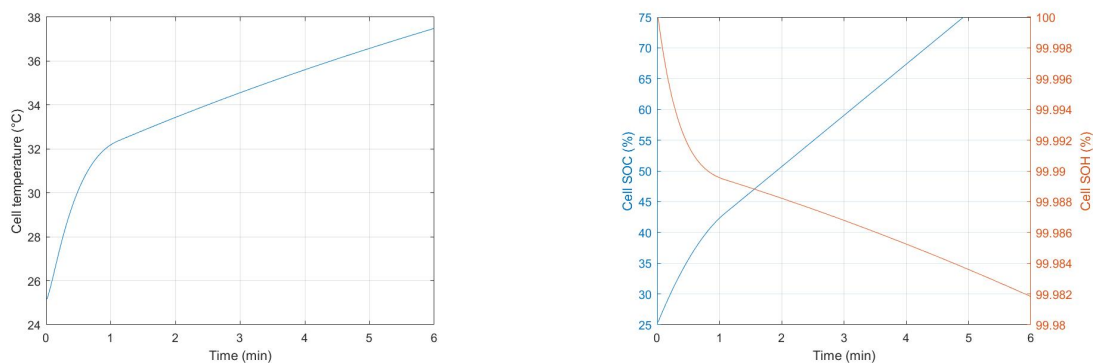


**Figure 7.15:** Temperature, SOC and voltage evolution for the replicated test.

### 7.3 Battery pack

A test of the model is performed simulating a battery pack. The number of cells is computed to reproduce the total energy of about 75 kWh. Generally battery packs are able to store a quantity of energy that goes from 20 kWh in case of small city cars, to more than 120 kWh, such as in big SUVs and luxury sedan vehicles.

Supposing a battery pack voltage of 375 V and knowing the terminal voltage and capacity of each of the cells, that are 3.3 V and 2.05 Ah, the number of cell to be connected in parallel and those to be connected in series are computed. Using the equations reported in section 5.1.1, the ratio between the battery pack voltage and the nominal voltage of a single cell returns the number of cells connected in series. From the equation of the energy of a battery pack, the number of cells connected in parallel is found.

The battery pack results constituted of a parallel of 97 cells, which are put together in a series of 114 PCM.

The model is able to simulate every single cell of the pack, returning for each the voltage behavior, temperature evolution and cell degradation with respect to the SOC.

In this work, the cell balancing has not been implemented. For this reason all the cells will behave in the same way.

Moreover the cells are supposed to be identical, so they do not present differences in the composition and construction of the components. The equivalent parameters of the circuit that represents the cell are equal and the same current will flow through each of the cells. For this reason the voltage behavior and the other output of the model are equal for all the cells.

A simulation is conducted for the battery pack, with a charging current intensity of 1C and under temperature condition of 25 °C.

The reported outcome in figure 7.16 is the SOC variation of the battery pack, that is calculated as the average of the SOC of all the cells. The charging power, considering 1C for the current intensity, 375 V for the pack voltage and considering 114 cell connected in series and 97 in parallel, is about 75 kW. Since the current intensity is very low, the time is not enough to fully charge the battery pack.

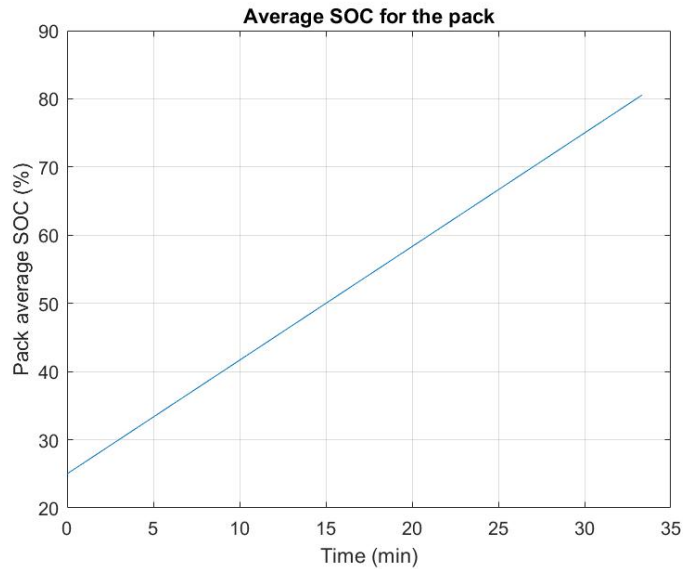


**Figure 7.16:** SOC variation during 1C charging simulation at 25 °C for the battery pack.

## 7.4 Future works

The model can be improved by introducing some considerations:

- a better method for estimating the SOC and consequently obtain a more reliable model,
- a system to equalize the energy contained in the cells of the battery pack,
- a controller for preserving battery life without impacting on the best charging time.

### 7.4.1 Kalman filters for SOC and SOH estimation

The rough methods to evaluate the SOC can lead to errors in the estimation of all the variables of the state of the system, because dependent on the estimation of the initial SOC and on the current, that is affected by noise and measurement bias. First a better algorithm for estimating the cell SOC can be implemented. The basis of the work is introduced in section 5.3.

A similar approach can be applied to the estimation of the SOH. The parameters are predicted and the error covariance is updated, then the estimator gain matrix is computed to update the parameter estimation and finally the error covariance of the parameter estimation is updated. A simultaneous prediction of cell parameters

and state of the dynamic system can be performed, then the steps of the Kalman filter methods can be applied.

### 7.4.2 Balancing of pack cells

Battery cells do not behave identical. Even very little differences in the composition of the electrodes or in the production process, result in slightly different capacity or voltage behavior and consequently in different equivalent parameters of the ECM. Some cells can be weaker than the others. This means that their Coulombic efficiencies are lower, so a smaller fraction of the charging current is converted into stored energy. The SOC will be different with respect the stronger cells. Also charging current itself might be not equal for all the cells, because of different self-discharge and leakage behavior. If the same current is applied to all the cells, the stronger cells can experience overcharging during charging process, while the weaker cells can overdischarge when energy is released.

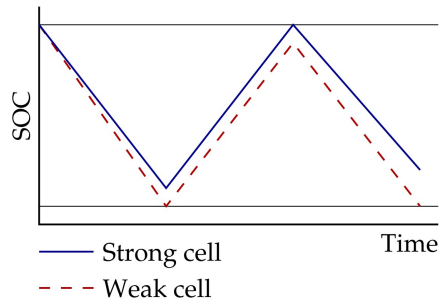


**Figure 7.17:** SOC evolution with imbalanced cells.

A good cell SOC estimator is necessary for an efficient balancing strategy, otherwise the balancing circuit can operate on the wrong cell, causing further imbalance.

Passive circuits use resistors to dissipate the excess energy stored in stronger cells, in order to equalize the charge of all the cells. A non-dissipative strategy is for instance to rely on the total energy that can be delivered by each cell. The energy that is stored in stronger cells is distributed among those cells for which the stored energy is lower.

### 7.4.3 Charging strategies and control

A specific controller can be coupled to the thermal-aging-electrical model. While simply charging at the maximum allowed C-rate enables the reduction of charging times, the battery can suffer some degradation because of the stress it is subjected

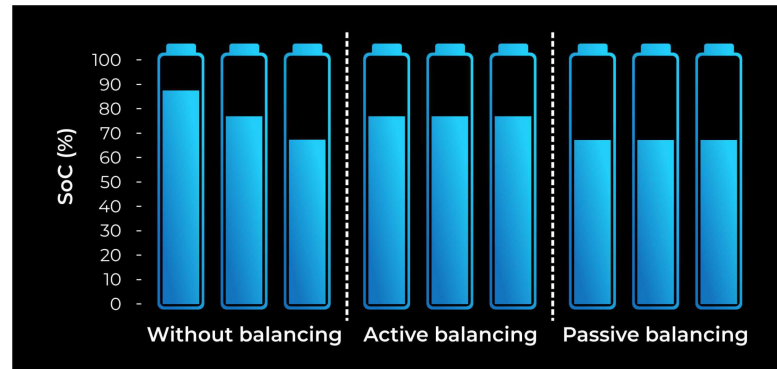


**Figure 7.18:** Balancing strategy for battery pack cells [66].

to. The temperature increase, that is more important as the charging power increases, lead to an accelerated degradation of the electrodes.

For these reasons an algorithm that performs a control of the charging time and capacity loss, is necessary to balance the two factors. Beside the rough minimization of the charging time, generally performed pushing the maximum current in the CC-CV logic, the target can be to minimize the aging of the cell or to find a trade off of the two.

When the period during which a vehicle is plugged in is higher than the time required to restore 100 % of the SOC, so when fast charge is not required, some protocols can be applied to preserve the maximum possible SOH. Degradation can be highly mitigated, as in [67] a reduction of 46.2 % of the degradation for a single cycle is achieved.

On the other hand, when a rapid charging is required, some algorithms are able to achieve an optimal tradeoff between charging time and degradation.

Multistage constant current strategy employs different current levels. The cell undergoes CC charging at a high level, until the maximum voltage of the cell is reached. At this point the current intensity is switched to a lower level, that is hold as long as the cell voltage is lower than the maximum, and so on. A reduction in charging time of 34.2 % employing the multilevel current strategy is reported in [69].

More sophisticated algorithms are able to control in real time the actors of the cell model, to achieve a significantly lower SOH decay with respect to the minimum-time protocol, with an almost imperceptible increase of time, as in [64].

A multi-objective function is implemented combining the charging time and degradation. The weighting factor defines the extreme prevalence of one of the two objective over the other or performs a swing between the two, for achieving the optimal trade-off.

Finally it increases up to the moment in which the current is stopped. At this

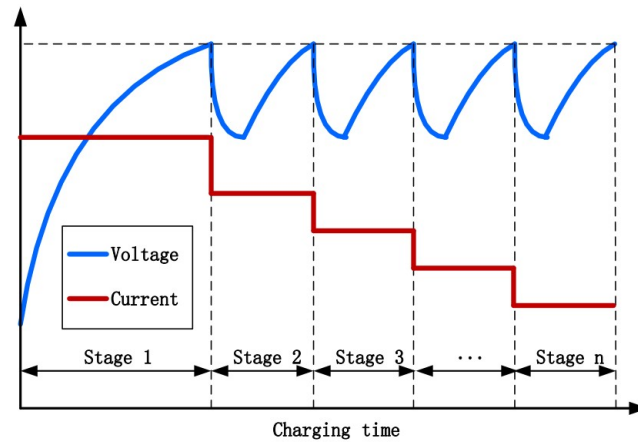


**Figure 7.19:** Multilevel constant current charging strategy [68].

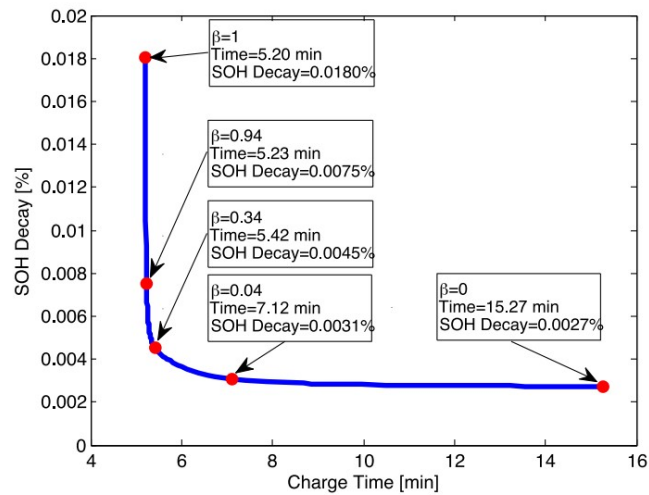


**Figure 7.20:** Pareto frontier to evaluate the incidence of the weighting factor on charging time and degradation [64].

point the cell voltage drops, because of the absence of current through the cell components.

The voltage drop due to the ohmic resistance is clearly visible in correspondence of the current stop. Right after, the diffusion voltages present a relaxation of the voltage curve.

# Chapter 8

## Conclusions

The aim of this work was to build a model of battery cell capable of simulating the voltage behavior and SOC evolution during the charging process.

An equivalent circuit model (ECM) is selected for modeling the electrical behavior of the cell. The simplicity of construction, the not high computational power and time required and the relative ease in acquiring the needed information about the cell, turned the ECM preferable to the PBM.

The temperature variation due to the current flowing through the cell affects the parameters of the cell. To improve the model accuracy, the thermal model of the cell is implemented. The output is the temperature of the core of the cell.

Moreover the temperature affects the aging of the cell, together with the current intensity that is applied to the cell. A model for computing the degradation of the cell considering the operating conditions is presented and integrated together with the electrical and thermal ones.

The critical point of the work, was the total lack of information about any cell. No database or testing equipment to collect data on one or more cell models were available. For this reason the complete model is tested using data accessible on the web.

The test performed by the model, replicating the conditions of some experiments reported in articles, returns values for the temperature evolution, voltage behavior and even state of charge decrease very close to the results of the articles.

The goodness of the model is demonstrated by the match between the plots of the two cases and their values.

The model is capable to simulate a battery pack, selecting the number of cells in series and in parallel. The appreciable result is trivial, since the cells are supposed to behave identically, both regarding temperature variation and voltage evolution.

The model can be further improved by implementing a more reliable estimation of the SOC and SOH, for instance through the use of Kalman filter. An algorithm to equalize the charge stored in all the cells of a battery pack can be included.

Finally a controller can be developed, with the aim of finding the optimal trade-off between charging time and capacity loss.

# Appendix A

## Matlab scripts

### A.1 Open circuit voltage and ohmic resistance

The code is used to extract and plot the OCV vs SOC relation and the variation of the internal resistance for different temperatures, again with respect to the SOC.

```
1 % load the database of the selected cell model
2 load A123model.mat; % creates var. "model" with A123 cell
   parameter values
3
4 % extract the value of OCV of the cell for the selected
   temperature from the dataset
5 v_store=zeros(100,1);
6 for z=1:100
7     v_store(z)=OCVfromSOCtemp(z/100,25,model);
8 end
9 % plot the variation of OCV with respect to SOC
10 figure
11 plot((1:100)/100,v_store)
12 xticks(0:0.5:1)
13 xlim([0 1])
14 ylim([2 4])
15 xlabel('SOC'); ylabel('OCV (V)');
16 title('Relation between OCV and SOC');
17
18 % extract the values of the internal resistance of the cell for
   the different temperatures from the dataset
19 r0_store=NaN(100,5);
20 T=[5 15 25 35 45]';
21 for k=1:5
22     for z=10:95
23         r0_store(z,k)=getParamESC('R0Param',T(k),model);
```

```

24     end
25 end
26 % plot the variation of ohmic resistance with temperature
27 figure
28 plot((1:100)/100,r0_store)
29 xticks(0:0.5:1)
30 xlim([0 1])
31 ylim([0.005 0.02])
32 legend('5 °C','15 °C','25 °C','35 °C','45 °C')
33 xlabel('SOC'); ylabel('R_0 (\Omega)');
34 title('Ohmic resistance variation with SOC for different
    temperatures');

```

## A.2 Thermal-aging-electrical model

```

1 % Code to simulate a single cell or a complete battery pack, with
  % selectable number of cells in parallel and in series.
2 The code includes the thermal model, the degradation model and the
  % electrical model of the cell.
3
4 clear all; close all; clc;
5
6 % load cell model and select number of cells in series and in
  % parallel
7 load A123model.mat; % load cell model in the variable "model"
8 Ns = 1; % number of modules connected in series to make a
  % pack
9 Np = 1; % number of cells connected in parallel in each
  % module
10
11 % allocate memory for some vectors
12 maxtime = 2000; % set simulation time
13 %t0 = 2700; % pack rests after time t0
14 storez = zeros([maxtime Ns Np]); % create storage for SOC
15 storei = zeros([maxtime Ns Np]); % create storage for current
16 storeT = zeros([maxtime Ns Np]); % create storage for
  % temperature
17 irc = zeros(Ns,Np);
18 h = zeros(Ns,Np);
19 storeP = zeros([maxtime Ns Np]); % create storage for thermal
  % power
20 storer0 = zeros([maxtime Ns Np]); % create storage for ohmic
  % resistance
21 storer = zeros([maxtime Ns Np]); % create storage for diffusion
  % resistance

```

```

22 v_temp = zeros(maxtime,1);           % create storage for voltage
23 avgSOC = zeros(maxtime,1);
24
25 % set charging range - min and max SOC
26 z      = 0.25*ones(Ns,Np); % initialize SOC at 25 %
27 z_stop = 0.95; % set SOC at which charging stops
28
29 Temp = 25; % set initial core temperature in °C
30
31 q      = getParamESC('QParam',Temp,model)*ones(Ns,Np);
32         % extract cell capacity
33 rc     = exp(-1./abs(getParamESC('RCParam',Temp,model)))'*ones(Ns,Np
34         );
35         % extract time constant
36 r      = (getParamESC('RParam',Temp,model))';
37         % extract cell diffusion resistance
38 m      = getParamESC('MParam',Temp,model)*ones(Ns,Np);
39         % extract hysteresis parameter
40 g      = getParamESC('GParam',Temp,model)*ones(Ns,Np);
41 r0     = getParamESC('ROParam',Temp,model)*ones(Ns,Np);
42         % extract cell ohmic resistance
43 rt     = 0.000125; % 125 microOhm resistance for each tab
44
45 m = 0*m; % eliminate model hysteresis for rough simulation
46
47 % compute pack capacity in Ah
48 totalCap = min(sum(q,2)); % pack capacity = minimum module
49           capacity
50
51 C_r      = 5;           % initial C-rate
52 I        = -C_r*totalCap; % pack current
53
54 % thermal model data
55 % -----
56 t=1;           % time step for thermal model iterations
57 R_c = 1.94;    % heat conduction (cell) resistance K/W
58 R_u = 3.08;    % heat convection (air) resistance K/W
59 C_c = 62.7;    % core (cell) heat capacity J/K
60 C_s = 4.5;     % surface heat capacity J/K
61
62 T_amb      = 298.15;    % ambient temperature in K
63 T_core_p   = Temp + 273.15; % internal cell temp initial condition
64           in K
65 T_cell_p   = 298.15;    % surface cell temp initial condition
66           in K
67
68 % aging model data
69 % -----
70 SOH        = ones(maxtime,1); % initialize state of health at 100 %

```

```

66 deltaQ = 20; % end of life set at 80 % of nominal
    capacity
67 R = 8.314; % gas constant J/mol/K
68 DoD_cycles = z_stop-z(1,1); % depth of discharge for computing
    aging
69
70 % add faults to pack: cells faulted open- and short-circuit
71 Rsc = 0.0025; % resistance value to use for cell whose SOC < 0%
72
73 T=25;
74 time=(1:maxtime);
75
76 % Simulate pack performance using ESC cell model.
77 % First compute thermal power resulting from the current flowing
    through resistances (Joule effect)
78 % Run the thermal model, where the inputs are the heat generated
    by the cell and the power dissipated to the cooling fluid; the
    output is the temperature of the core of the cell
79 % Update all the cell parameters according to the computed cell
    temperature. The cell SOC is updated according to the current
    that flows inside/outside the battery
80 % Then the aging model is run, where the SOH of the cell is
    computed considering the actual cell temperature and current
    intensity, because they are the most critical factors when
    dealing with cell degradation.
81
82 for k = 1:maxtime
83
84     % thermal model
85     P_th = r0(1,1)*I^2+r(1,1)*irc(1,1)^2; % thermal power
    generation, considering both ohmic resistance and diffusion
    resistance
86     u = P_th; % input to simulink model
87     storeP(k, :, :) = P_th; % store thermal power
88
89     sim('fun_sim_5_2.slx'); % call simulink model
90
91     T=ans.yout{1}.Values.Data(51)-273.15; % acquire temperature
    from simulink model to put as input for data acquisition
92
93     % update all cell parameters with temperature variation
94     rc = exp(-1./abs(getParamESC('RCParam',T,model)))'*ones(Ns,
    Np);
95     r = (getParamESC('RParam',T,model))';
96     m = getParamESC('MParam',T,model)*ones(Ns,Np);
97     g = getParamESC('GParam',T,model)*ones(Ns,Np);
98     r0 = getParamESC('ROParam',T,model)*ones(Ns,Np);
99     rt = 0.000125; % 125 microOhm resistance for each tab
100

```

```

101     v = OCVfromSOCtemp(z,T,model); % extract cell OCV from
102     relation with SOC at defined T
103     v = v + m.*h - r.*irc; % add in capacitor voltages
104     and hysteresis
105     r0(isnan(z)) = Rsc; % short-circuit fault has "
106     short-circuit" resistance
107     V = (sum(v./r0,2) - I)./sum(1./r0,2);
108     ik = (v-repmat(V,1,Np))./r0;
109
110     z = z - (1/3600)*ik./q; % update each cell SOC
111     z(z<0) = NaN; % set over-discharged cells to
112     short-circuit fault
113     irc = rc.*irc + (1-rc).*ik; % update capacitor voltages
114     fac = exp(-abs(g.*ik)./(3600*q));
115     h = fac.*h + (1-fac).*sign(ik); % update hysteresis voltages
116
117     minz = min(z(:)); maxz = max(z(:)); % check to see if SOC
118     limit hit
119     % if minz < 0.05, I = -abs(I); end % stop discharging
120     % if maxz > 0.95, I = abs(I); end % stop charging
121     if maxz > z_stop, I = 0; end % stop charging when SOC is 95 %
122     % if k>t0, I = 0; end % rest
123
124     storez(k,:,:)= z; % store SOC for later plotting
125     storei(k,:,:)= ik; % store current for later plotting
126     storer0(k,:,:)= r0; % store ohmic resistance
127     storer(k,:,:)= r; % store resistance of rc branch
128     C = abs(I)/q; % update C-rate for SOH computation
129
130     T_core_p = ans.yout{1}.Values.Data(51); % update core T as
131     initial condition
132     T_cell_p = ans.yout{2}.Values.Data(51); % update surface T
133     as initial condition
134
135     if T<25
136         T = 25;
137     end
138
139     storeT(k,:,:)= T; % store computed temperature of
140     the core of the cell
141     v_temp(k) = v(1,1);
142
143     % aging model
144     if k>1

```

```

139     % the parameters of the aging model vary according to the
140     C-rate, so for each parameter the set of values are
141     interpolated to find the actual value correspondent to the
142     applied current intensity
143
144     C_rates = [1/2, 2, 6, 10];
145
146     % interpolation for pre-exponential factor
147     B_vec = [30330, 19300, 12000, 11500];
148     B_loss = interp1(C_rates,B_vec,C,'pchip');
149
150     % interpolation for activation energy
151     E_a_vec = [31500, 31000, 29500, 28000];
152     E_a = interp1(C_rates,E_a_vec,C,'pchip');
153
154     % interpolation for exponential factor
155     z_vec = [0.552, 0.554, 0.56, 0.56];
156     z_loss = interp1(C_rates,z_vec,C,'pchip');
157
158     % compute the total charge quantity that can be extracted
159     from or put inside the cell considering the C-rate and
160     temperature and preserving 80 % of the total capacity of the
161     cell
162
163     A_thr = (deltaQ/(B_loss*exp(-E_a/R/T_core_p)))^(1/z_loss);
164     % total Ah throughput
165
166     N = A_thr/q/DoD_cycles; % number of cycles at the EOL
167
168     SOH(k) = SOH(k-1)-C/(2*N*3600); % state of health update
169
170 end
171
172 % make SOC avg for battery pack
173 avgSOC(k) = mean(mean(z));
174
175 if I ~= 0
176     stop_t = k; % time at which stop charging
177 end
178 end % for k
179
180 % plot some of the collected data from the simulation
181
182 if Ns == 1 && Np == 1
183     % plot SOC for the cell
184     figure(1); clf; plot((1:maxtime)/60,avgSOC*100); grid on
185     xlabel('Time (min)'); ylabel('Cell SOC (%)');
186     title('Cell state of charge (SOC) variation during charging');

```

```
181 else
182     % plot avgSOC for the battery pack
183     figure(1); clf; plot((1:maxtime)/60,avgSOC*100); grid on
184     xlabel('Time (min)'); ylabel('Pack average SOC (%)');
185     title('Average SOC for the pack');
186 end
187
188 % plot cell temperature
189 figure(2); clf; plot((1:maxtime)/60,storeT); grid on
190 xlabel('Time (min)'); ylabel('Cell temperature (°C)');
191 %title('Variation of the cell temperature during charging');
192
193 % plot SOH variation
194 figure(3); clf; plot((1:maxtime)/60,SOH*100); grid on
195 xlabel('Time (min)'); ylabel('Cell SOH (%)');
196 %title('Variation of the cell state of health during charging');
197
198 % plot cell terminal voltage
199 figure(4); clf; plot((1:maxtime)/60,v_temp); grid on
200 xlabel('Time (min)'); ylabel('Cell terminal voltage (V)');
201 %title('Variation of the cell terminal voltage during charging');
202
203 % plot ohmic resistance
204 figure(5); clf; plot((1:maxtime)/60,storer0(:,1,1)*1000); grid on
205 xlabel('Time (min)'); ylabel('Cell ohmic resistance (m\Omega)');
206 %title('Variation of the cell internal (ohmic) resistance during
207         charging');
208
209 % plot SOC and voltage on the same graph
210 figure(6); clf;
211 yyaxis right
212 plot((1:maxtime)/60,v_temp); grid on
213 ylabel('Cell terminal voltage (V)');
214 yyaxis left
215 plot((1:maxtime)/60,avgSOC*100);
216 ylabel('Cell SOC (%)');
217 xlabel('Time (min)');
218 %title('Variation of SOC and cell terminal voltage during charging
219         ');
```

# Bibliography

- [1] IEA. *Energy Technology Perspectives 2020*. [Online]. 2020. URL: <https://www.iea.org/reports/energy-technology-perspectives-2020> (cit. on p. 1).
- [2] IEA. *Transport sector CO2 emissions by mode in the Sustainable Development Scenario, 2000-2030*. [Online]. 2022. URL: <https://www.iea.org/data-and-statistics/charts/transport-sector-co2-emissions-by-mode-in-the-sustainable-development-scenario-2000-2030> (cit. on p. 1).
- [3] IEA. *Electric cars fend off supply challenges to more than double global sales*. [Online]. 2022. URL: <https://www.iea.org/commentaries/electric-cars-fend-off-supply-challenges-to-more-than-double-global-sales> (cit. on p. 1).
- [4] Muhammad Shafique, Anam Azam, Muhammad Rafiq, and Xiaowei Luo. «Life cycle assessment of electric vehicles and internal combustion engine vehicles: A case study of Hong Kong». In: *Research in Transportation Economics* (2021), p. 101112. ISSN: 0739-8859. DOI: <https://doi.org/10.1016/j.retrec.2021.101112> (cit. on p. 1).
- [5] Quentin Hoarau and Etienne Lorang. «An assessment of the European regulation on battery recycling for electric vehicles». In: *Energy Policy* 162 (2022), p. 112770. ISSN: 0301-4215. DOI: <https://doi.org/10.1016/j.enpol.2021.112770> (cit. on p. 2).
- [6] Pei-Hsing Huang, Jenn-Kun Kuo, and Chun-Yen Huang. «A new application of the UltraBattery to hybrid fuel cell vehicles». In: *International Journal of Energy Research* 40 (Jan. 2015). DOI: [10.1002/er.3426](https://doi.org/10.1002/er.3426) (cit. on p. 5).
- [7] *Standard Reduction Potentials by Value*. [Online]. Dec. 2021 (cit. on p. 5).
- [8] A. Rufer. *Energy Storage: Systems and Components*. CRC Press, 2017. ISBN: 9781351621939 (cit. on p. 5).

- [9] Soon-Jong Kwon, Sung-Eun Lee, Ji-Hun Lim, Jinhyeok Choi, and Jonghoon Kim. «Performance and Life Degradation Characteristics Analysis of NCM LIB for BESS». In: *Electronics* 7.12 (2018). ISSN: 2079-9292. DOI: 10.3390/electronics7120406 (cit. on p. 7).
- [10] Christian M. Julien, Alain Mauger, Karim Zaghib, and Henri Groult. «Comparative Issues of Cathode Materials for Li-Ion Batteries». In: *Inorganics* 2.1 (2014), pp. 132–154. ISSN: 2304-6740. DOI: 10.3390/inorganics2010132 (cit. on pp. 8, 36).
- [11] T. Richard Jow, Kang Xu, Oleg Borodin, Makoto Ue. *Electrolytes for Lithium and Lithium-Ion Batteries*. Springer, 2014. ISBN: 978-1-4939-0302-3 (cit. on p. 7).
- [12] Sheng Shui Zhang. «A review on electrolyte additives for lithium-ion batteries». In: *Journal of Power Sources* 162.2 (2006), pp. 1379–1394. ISSN: 0378-7753. DOI: <https://doi.org/10.1016/j.jpowsour.2006.07.074> (cit. on p. 7).
- [13] Gregory Plett. *Battery Management Systems, Volume I: Battery Modeling*. 2015 (cit. on pp. 8, 16, 17, 20, 25).
- [14] Diego E. Galvez-Aranda, Victor Ponce, and Jorge M. Seminario. «Molecular dynamics simulations of the first charge of a Li-ion—Si-anode nanobattery». In: 23.4 (Mar. 2017). ISSN: 1610-2940. DOI: 10.1007/s00894-017-3283-2 (cit. on p. 9).
- [15] Wenming Li, Wendi Chen, Hui Zhang, and Zhongyi Zhang. «Integratable solid-state zinc-air battery with extended cycle life inspired by bionics». In: *Chemical Engineering Journal* 435 (2022), p. 134900. ISSN: 1385-8947. DOI: <https://doi.org/10.1016/j.cej.2022.134900> (cit. on p. 9).
- [16] A. Pradel and M. Ribes. «7 - Ionic conductivity of chalcogenide glasses». In: *Chalcogenide Glasses*. Ed. by Jean-Luc Adam and Xianghua Zhang. Woodhead Publishing, 2014, pp. 169–208. ISBN: 978-0-85709-345-5. DOI: <https://doi.org/10.1533/9780857093561.1.169> (cit. on p. 9).
- [17] *Electric-Powered Vehicles: Electrolyte Spillage and Electrical Shock Protection*. [Online]. Sept. 2017. URL: <https://www.federalregister.gov/documents/2017/09/27/2017-20350/federal-motor-vehicle-safety-standards-electric-powered-vehicles-electrolyte-spillage-and-electrical> (cit. on p. 13).
- [18] Gregory Plett. *Battery Management Systems, Volume II: Equivalent-Circuit Methods*. 2015 (cit. on pp. 14, 30, 31, 35).

- [19] Michael Roscher, Oliver Bohlen, and Jens Vetter. «OCV Hysteresis in Li-Ion Batteries including Two-Phase Transition Materials». In: *SAGE-Hindawi Access to Research International Journal of Electrochemistry Article ID 984320* (May 2011). DOI: 10.4061/2011/984320 (cit. on p. 17).
- [20] Linfeng Zheng, Lei Zhang, Jianguo Zhu, Guoxiu Wang, and Jiuchun Jiang. «Co-estimation of state-of-charge, capacity and resistance for lithium-ion batteries based on a high-fidelity electrochemical model». In: *Applied Energy* 180 (2016), pp. 424–434. ISSN: 0306-2619. DOI: <https://doi.org/10.1016/j.apenergy.2016.08.016> (cit. on p. 18).
- [21] Alexander Bartlett, James Marcicki, Simona Onori, Giorgio Rizzoni, Xiao Guang Yang, and Ted Miller. «Electrochemical Model-Based State of Charge and Capacity Estimation for a Composite Electrode Lithium-Ion Battery». In: *IEEE Transactions on Control Systems Technology* 24.2 (2016), pp. 384–399. DOI: 10.1109/TCST.2015.2446947 (cit. on p. 18).
- [22] Sangwoo Han, Yifan Tang, and Saeed Khaleghi Rahimian. «A numerically efficient method of solving the full-order pseudo-2-dimensional (P2D) Li-ion cell model». In: *Journal of Power Sources* 490 (2021), p. 229571. ISSN: 0378-7753. DOI: <https://doi.org/10.1016/j.jpowsour.2021.229571> (cit. on p. 18).
- [23] Meng Xu, Rui Wang, Peng Zhao, and Xia Wang. «Fast charging optimization for lithium-ion batteries based on dynamic programming algorithm and electrochemical-thermal-capacity fade coupled model». In: *Journal of Power Sources* 438 (2019), p. 227015. ISSN: 0378-7753. DOI: <https://doi.org/10.1016/j.jpowsour.2019.227015> (cit. on pp. 21, 22).
- [24] James L. Lee, Andrew Chemistruck, and Gregory L. Plett. «One-dimensional physics-based reduced-order model of lithium-ion dynamics». In: *Journal of Power Sources* 220 (2012), pp. 430–448. ISSN: 0378-7753. DOI: <https://doi.org/10.1016/j.jpowsour.2012.07.075>. URL: <https://www.sciencedirect.com/science/article/pii/S0378775312012104> (cit. on pp. 21, 22).
- [25] Bharatkumar Suthar, Paul W. C. Northrop, Richard D. Braatz, and Venkat R. Subramanian. «Optimal Charging Profiles with Minimal Intercalation-Induced Stresses for Lithium-Ion Batteries Using Reformulated Pseudo 2-Dimensional Models». In: *Journal of The Electrochemical Society* 161.11 (2014), F3144–F3155. DOI: 10.1149/2.0211411jes (cit. on p. 22).
- [26] Yanqing Lai, Shuanglong Du, Liang Ai, Lihua Ai, Yun Cheng, Yiwei Tang, and Ming Jia. «Insight into heat generation of lithium ion batteries based on the electrochemical-thermal model at high discharge rates». In: *International*

- Journal of Hydrogen Energy* 40.38 (2015), pp. 13039–13049. ISSN: 0360-3199. DOI: <https://doi.org/10.1016/j.ijhydene.2015.07.079> (cit. on p. 22).
- [27] Manuel Antonio Perez Estevez, Sandro Calligaro, Omar Bottesi, Carlo Caligiuri, and Massimiliano Renzi. «An electro-thermal model and its electrical parameters estimation procedure in a lithium-ion battery cell». In: *Energy* 234 (2021), p. 121296. ISSN: 0360-5442. DOI: <https://doi.org/10.1016/j.energy.2021.121296> (cit. on pp. 22, 27).
- [28] Hongwen He, Rui Xiong, Hongqiang Guo, and Shuchun Li. «Comparison study on the battery models used for the energy management of batteries in electric vehicles». In: *Energy Conversion and Management* 64 (2012). IREC 2011, The International Renewable Energy Congress, pp. 113–121. ISSN: 0196-8904. DOI: <https://doi.org/10.1016/j.enconman.2012.04.014> (cit. on p. 22).
- [29] Karl Löffler, Raghavendra Arunachala, Sabine Arnold, Hassen Ennifar, Han Zhou, Andreas Jossen, and Wen Changyun. «A Lumped Electro-Thermal Model for Li-Ion Cells in Electric Vehicle Application». In: *World Electric Vehicle Journal* 7 (Mar. 2015), pp. 1–13. DOI: [10.3390/wevj7010001](https://doi.org/10.3390/wevj7010001) (cit. on pp. 22, 27).
- [30] Ruijia Fan, Caizhi Zhang, Yi Wang, Chenzhen Ji, Zaiqiang Meng, Lei Xu, Yang Ou, and Cheng Siong Chin. «Numerical study on the effects of battery heating in cold climate». In: *Journal of Energy Storage* 26 (2019), p. 100969. ISSN: 2352-152X. DOI: <https://doi.org/10.1016/j.est.2019.100969> (cit. on p. 24).
- [31] T.D. Nguyen, J. Deng, B. Robert, W. Chen, and T. Siegmund. «Experimental investigation on cooling of prismatic battery cells through cell integrated features». In: *Energy* 244 (2022), p. 122580. ISSN: 0360-5442. DOI: <https://doi.org/10.1016/j.energy.2021.122580> (cit. on pp. 25, 27).
- [32] Antti Väyrynen and Justin Salminen. «Lithium ion battery production». In: *The Journal of Chemical Thermodynamics* 46 (2012). Thermodynamics of Sustainable Processes, pp. 80–85. ISSN: 0021-9614. DOI: <https://doi.org/10.1016/j.jct.2011.09.005> (cit. on p. 25).
- [33] *Numerical Investigation of Thermal Properties for Li-Ion Battery*. Vol. ASME 2020 Heat Transfer Summer Conference. Heat Transfer Summer Conference. V001T02A005. July 2020. DOI: [10.1115/HT2020-9108](https://doi.org/10.1115/HT2020-9108). URL: <https://doi.org/10.1115/HT2020-9108> (cit. on p. 25).
- [34] Yan Zhao, Laura Bravo Diaz, Yatish Patel, Teng Zhang, and Gregory Offer. «How to Cool Lithium Ion Batteries: Optimising Cell Design using a Thermally Coupled Model». In: *Journal of The Electrochemical Society* 166 (Jan. 2019), A2849–A2859. DOI: [10.1149/2.0501913jes](https://doi.org/10.1149/2.0501913jes) (cit. on p. 25).

- [35] Stephen J. Bazinski and Xia Wang. «Experimental study on the influence of temperature and state-of-charge on the thermophysical properties of an LFP pouch cell». In: *Journal of Power Sources* 293 (2015), pp. 283–291. ISSN: 0378-7753. DOI: <https://doi.org/10.1016/j.jpowsour.2015.05.084> (cit. on p. 25).
- [36] S.S. Zhang, K. Xu, and T.R. Jow. «The low temperature performance of Li-ion batteries». In: *Journal of Power Sources* 115.1 (2003), pp. 137–140. ISSN: 0378-7753. DOI: [https://doi.org/10.1016/S0378-7753\(02\)00618-3](https://doi.org/10.1016/S0378-7753(02)00618-3). URL: <https://www.sciencedirect.com/science/article/pii/S0378775302006183> (cit. on p. 26).
- [37] Zhiguo Lei, Yuwen Zhang, and Xueguo Lei. «Improving temperature uniformity of a lithium-ion battery by intermittent heating method in cold climate». In: *International Journal of Heat and Mass Transfer* 121 (2018), pp. 275–281. ISSN: 0017-9310. DOI: <https://doi.org/10.1016/j.ijheatmasstransfer.2017.12.159>. URL: <https://www.sciencedirect.com/science/article/pii/S0017931017341996> (cit. on p. 26).
- [38] *Battery cooling*. [Online]. URL: <https://www.emobility-engineering.com/ev-battery-cooling/> (cit. on p. 26).
- [39] Vima Mali, Rajat Saxena, Kundan Kumar, Abul Kalam, and Brijesh Tripathi. «Review on battery thermal management systems for energy-efficient electric vehicles». In: *Renewable and Sustainable Energy Reviews* 151 (2021), p. 111611. ISSN: 1364-0321. DOI: <https://doi.org/10.1016/j.rser.2021.111611>. URL: <https://www.sciencedirect.com/science/article/pii/S136403212100887X> (cit. on p. 27).
- [40] Joris De Hoog, Joris Jaguemont, Mohamed Abdel-Monem, Peter Van Den Bossche, Joeri Van Mierlo, and Noshin Omar. «Combining an Electrothermal and Impedance Aging Model to Investigate Thermal Degradation Caused by Fast Charging». In: *Energies* 11.4 (2018). ISSN: 1996-1073. DOI: [10.3390/en11040804](https://doi.org/10.3390/en11040804). URL: <https://www.mdpi.com/1996-1073/11/4/804> (cit. on p. 27).
- [41] Guanchen Liu and Lijun Zhang. «Research on the Thermal Characteristics of an 18650 Lithium-Ion Battery Based on an Electrochemical-Thermal Flow Coupling Model». In: *World Electric Vehicle Journal* 12.4 (2021). ISSN: 2032-6653. DOI: [10.3390/wevj12040250](https://doi.org/10.3390/wevj12040250). URL: <https://www.mdpi.com/2032-6653/12/4/250> (cit. on p. 28).
- [42] Mohammad Shahjalal, Probir Kumar Roy, Tamanna Shams, Ashley Fly, Jahedul Islam Chowdhury, Md. Rishad Ahmed, and Kailong Liu. «A review on second-life of Li-ion batteries: prospects, challenges, and issues». In: *Energy*

- 241 (2022), p. 122881. ISSN: 0360-5442. DOI: <https://doi.org/10.1016/j.energy.2021.122881> (cit. on p. 28).
- [43] Quentin Hoarau and Etienne Lorang. «An assessment of the European regulation on battery recycling for electric vehicles». In: *Energy Policy* 162 (2022), p. 112770. ISSN: 0301-4215. DOI: <https://doi.org/10.1016/j.enpol.2021.112770> (cit. on p. 28).
- [44] *Audi Opens Battery Storage Unit on Berlin EUREF Campus*. [Online]. 2019. URL: <https://www.audi-mediacycenter.com/en/press-releases/audi-opens-battery-storage-unit-on-berlin-euref-campus-11681> (cit. on p. 28).
- [45] R. Spotnitz. «Simulation of capacity fade in lithium-ion batteries». In: *Journal of Power Sources* 113.1 (2003), pp. 72–80. ISSN: 0378-7753. DOI: [https://doi.org/10.1016/S0378-7753\(02\)00490-1](https://doi.org/10.1016/S0378-7753(02)00490-1). URL: <https://www.sciencedirect.com/science/article/pii/S0378775302004901> (cit. on p. 29).
- [46] Hao Zhou, Yangyang Xie, Xianggang Gao, Zhiyong Chen, Hao Jiang, Yan Tong, Xinming Fan, Yanqing Lai, and Zhian Zhang. «The influence of water in electrodes on the solid electrolyte interphase film of micro lithium-ion batteries for the wireless headphone». In: *Journal of Colloid and Interface Science* 606 (2022), pp. 1729–1736. ISSN: 0021-9797. DOI: <https://doi.org/10.1016/j.jcis.2021.08.137>. URL: <https://www.sciencedirect.com/science/article/pii/S0021979721013655> (cit. on p. 30).
- [47] Chen Fang, Thanh-Nhan Tran, Yangzhi Zhao, and Gao Liu. «Electrolyte decomposition and solid electrolyte interphase revealed by mass spectrometry». In: *Electrochimica Acta* 399 (2021), p. 139362. ISSN: 0013-4686. DOI: <https://doi.org/10.1016/j.electacta.2021.139362>. URL: <https://www.sciencedirect.com/science/article/pii/S0013468621016522> (cit. on p. 30).
- [48] Shiwen Li, Chao Wang, Caixia Meng, Yanxiao Ning, Guohui Zhang, and Qiang Fu. «Electrolyte-dependent formation of solid electrolyte interphase and ion intercalation revealed by in situ surface characterizations». In: *Journal of Energy Chemistry* 67 (2022), pp. 718–726. ISSN: 2095-4956. DOI: <https://doi.org/10.1016/j.jechem.2021.10.003>. URL: <https://www.sciencedirect.com/science/article/pii/S2095495621005544> (cit. on p. 30).
- [49] Xianke Lin, Kavian Khosravinia, Xiaosong Hu, Ju Li, and Wei Lu. «Lithium Plating Mechanism, Detection, and Mitigation in Lithium-Ion Batteries». In: *Progress in Energy and Combustion Science* 87 (2021), p. 100953. ISSN: 0360-1285. DOI: <https://doi.org/10.1016/j.pecs.2021.100953>. URL: <https://www.sciencedirect.com/science/article/pii/S0360128521000953>

- [//www.sciencedirect.com/science/article/pii/S0360128521000514](http://www.sciencedirect.com/science/article/pii/S0360128521000514)  
(cit. on p. 30).
- [50] Zhanjun Guo and Zhiliang Chen. «High-temperature capacity fading mechanism for LiFePO<sub>4</sub>/graphite soft-packed cell without Fe dissolution». In: *Journal of Electroanalytical Chemistry* 754 (2015), pp. 148–153. ISSN: 1572-6657. DOI: <https://doi.org/10.1016/j.jelechem.2015.07.009>. URL: <https://www.sciencedirect.com/science/article/pii/S1572665715300126> (cit. on p. 31).
- [51] Gaizka Saldaña, José Ignacio San Martín, Inmaculada Zamora, Francisco Javier Asensio, Oier Oñederra, and Mikel González. «Empirical Electrical and Degradation Model for Electric Vehicle Batteries». In: *IEEE Access* 8 (2020), pp. 155576–155589. DOI: 10.1109/ACCESS.2020.3019477 (cit. on p. 31).
- [52] Alan Millner. «Modeling Lithium Ion battery degradation in electric vehicles». In: Oct. 2010, pp. 349–356. DOI: 10.1109/CITRES.2010.5619782 (cit. on p. 32).
- [53] Linfeng Zheng, Lei Zhang, Jianguo Zhu, Guoxiu Wang, and Jiuchun Jiang. «Co-estimation of state-of-charge, capacity and resistance for lithium-ion batteries based on a high-fidelity electrochemical model». In: *Applied Energy* 180 (2016), pp. 424–434. ISSN: 0306-2619. DOI: <https://doi.org/10.1016/j.apenergy.2016.08.016> (cit. on pp. 32, 34–36).
- [54] Yang Li, Mahinda Vilathgamuwa, San Shing Choi, Troy W. Farrell, Ngoc Tham Tran, and Joseph Teague. «Development of a degradation-conscious physics-based lithium-ion battery model for use in power system planning studies». In: *Applied Energy* 248 (2019), pp. 512–525. ISSN: 0306-2619. DOI: <https://doi.org/10.1016/j.apenergy.2019.04.143> (cit. on p. 32).
- [55] *What are the different capacity types?* [Online]. 2018. URL: <https://www.deweywaters.co.uk/nominal-capacity-vs-actual-usable-capacity-water-tank/> (cit. on p. 34).
- [56] Fan He, Xuesong Li, and Lin Ma. «Combined experimental and numerical study of thermal management of battery module consisting of multiple Li-ion cells». In: *International Journal of Heat and Mass Transfer* 72 (2014), pp. 622–629. ISSN: 0017-9310. DOI: <https://doi.org/10.1016/j.ijheatmasstransfer.2014.01.038>. URL: <https://www.sciencedirect.com/science/article/pii/S0017931014000660> (cit. on p. 46).
- [57] Xinhua Liu, Weilong Ai, Max Naylor Marlow, Yatish Patel, and Billy Wu. «The effect of cell-to-cell variations and thermal gradients on the performance and degradation of lithium-ion battery packs». In: *Applied Energy* 248 (2019), pp. 489–499. ISSN: 0306-2619. DOI: <https://doi.org/10.1016/j.apenergy>.

- 2019.04.108. URL: <https://www.sciencedirect.com/science/article/pii/S0306261919307810> (cit. on p. 46).
- [58] Deokhun Kang, Pyeong-Yeon Lee, Kisoo Yoo, and Jonghoon Kim. «Internal thermal network model-based inner temperature distribution of high-power lithium-ion battery packs with different shapes for thermal management». In: *Journal of Energy Storage* 27 (2020), p. 101017. ISSN: 2352-152X. DOI: <https://doi.org/10.1016/j.est.2019.101017>. URL: <https://www.sciencedirect.com/science/article/pii/S2352152X19305031> (cit. on p. 46).
- [59] Mohsen Akbarzadeh, Theodoros Kalogiannis, Joris Jaguemont, Jiacheng He, Lu Jin, Maitane Berecibar, and Joeri Van Mierlo. «Thermal modeling of a high-energy prismatic lithium-ion battery cell and module based on a new thermal characterization methodology». In: *Journal of Energy Storage* 32 (2020), p. 101707. ISSN: 2352-152X. DOI: <https://doi.org/10.1016/j.est.2020.101707>. URL: <https://www.sciencedirect.com/science/article/pii/S2352152X20315449> (cit. on p. 46).
- [60] D. Bernardi, E. Pawlikowski, and J. Newman. «A General Energy Balance for Battery Systems». In: *Journal of The Electrochemical Society* 132.1 (Jan. 1985), pp. 5–12. DOI: [10.1149/1.2113792](https://doi.org/10.1149/1.2113792). URL: <https://doi.org/10.1149/1.2113792> (cit. on pp. 46, 47).
- [61] Xinfan Lin, Hector E. Perez, Shankar Mohan, Jason B. Siegel, Anna G. Stefanopoulou, Yi Ding, and Matthew P. Castanier. «A lumped-parameter electro-thermal model for cylindrical batteries». In: *Journal of Power Sources* 257 (2014), pp. 1–11. ISSN: 0378-7753. DOI: <https://doi.org/10.1016/j.jpowsour.2014.01.097>. URL: <https://www.sciencedirect.com/science/article/pii/S0378775314001244> (cit. on p. 47).
- [62] John Wang, Ping Liu, Jocelyn Hicks-Garner, Elena Sherman, Souren Soukiazian, Mark Verbrugge, Harshad Tataria, James Musser, and Peter Finamore. «Cycle-life model for graphite-LiFePO<sub>4</sub> cells». In: *Journal of Power Sources* 196.8 (2011), pp. 3942–3948. ISSN: 0378-7753. DOI: <https://doi.org/10.1016/j.jpowsour.2010.11.134>. URL: <https://www.sciencedirect.com/science/article/pii/S0378775310021269> (cit. on pp. 49, 53).
- [63] I Bloom et al. «An accelerated calendar and cycle life study of Li-ion cells». In: *Journal of Power Sources* 101.2 (2001), pp. 238–247. ISSN: 0378-7753. DOI: [https://doi.org/10.1016/S0378-7753\(01\)00783-2](https://doi.org/10.1016/S0378-7753(01)00783-2). URL: <https://www.sciencedirect.com/science/article/pii/S0378775301007832> (cit. on p. 49).

- [64] Hector Eduardo Perez, Xiaosong Hu, Satadru Dey, and Scott J. Moura. «Optimal Charging of Li-Ion Batteries With Coupled Electro-Thermal-Aging Dynamics». In: *IEEE Transactions on Vehicular Technology* 66.9 (2017), pp. 7761–7770. DOI: 10.1109/TVT.2017.2676044 (cit. on pp. 52, 54, 60, 61, 65, 66).
- [65] Xianke Lin, Siyang Wang, and Youngki Kim. «A framework for charging strategy optimization using a physics-based battery model». In: *Journal of Applied Electrochemistry* 49 (Aug. 2019). DOI: 10.1007/s10800-019-01322-1 (cit. on pp. 52, 54, 56).
- [66] *How Does Cell Balancing Improve Battery Life*. [Online]. 2020. URL: <https://www.ionenergy.co/resources/blogs/cell-balancing-battery-life/> (cit. on p. 65).
- [67] Alberto Bocca, Alessandro Sassone, Alberto Macii, Enrico Macii, and Massimo Poncino. «An aging-aware battery charge scheme for mobile devices exploiting plug-in time patterns». In: *2015 33rd IEEE International Conference on Computer Design (ICCD)*. 2015, pp. 407–410. DOI: 10.1109/ICCD.2015.7357135 (cit. on p. 65).
- [68] Haitao Min, Weiyi Sun, Xinyong Li, Dongni Guo, Yuanbin Yu, Tao Zhu, and Zhongmin Zhao. «Research on the Optimal Charging Strategy for Li-Ion Batteries Based on Multi-Objective Optimization». In: *Energies* 10.5 (2017). ISSN: 1996-1073. DOI: 10.3390/en10050709. URL: <https://www.mdpi.com/1996-1073/10/5/709> (cit. on p. 66).
- [69] Mihir Gaglani, Rashmi Rai, and Soumitra Das. «Implementation Of Multilevel Battery Charging Scheme For Lithium-ion Batteries». In: *2019 National Power Electronics Conference (NPEC)*. 2019, pp. 1–6. DOI: 10.1109/NPEC47332.2019.9034748 (cit. on p. 65).